Universidade do Minho
Escola de Ciências

Pedro Branco Saldarriaga

Multi-scale fluvial remote sensing – A study on spatial scaling discrepancies between Sentinel-2 and UAV multispectral data on riparian zones in Northwest Portugal

março de 2022

Multi-scale fluvial remote sensing – A study on spatial scaling discrepancies between Sentinel-2 and UAV multispectral data on riparian zones in Northwest Portugal

Pedro Branco Saldarriaga

UMinho | 2022

Universidade do Minho
Escola de Ciências

Pedro Branco Saldarriaga

Multi-scale fluvial remote sensing – A study on spatial scaling discrepancies between Sentinel-2 and UAV multispectral data on riparian zones in Northwest Portugal

Dissertação de Mestrado

Mestrado em Biodiversidade, Ecologia e Alterações Globais

Trabalho efetuado sob a orientação do

Professor Doutor Renato Filipe Faria Henriques

e do

Doutor Giorgio Pace

~

março de 2022

AGRADECIMENTOS

Dado como terminado o processo de investigação e escrita da presente tese de mestrado, resta-me apenas escrever breves palavras de agradecimento a todos os que de uma maneira direta ou indireta me ajudaram a concluir este processo.

Primeiramente quero agradecer a ambos os professores orientadores por acreditarem nas minhas capacidades, pela ajuda fornecida ao longo destes 2 anos e pelo seu valioso contributo no desenvolvimento desta tese. Um especial agradecimento ao Professor Giorgio Pace pela constante disponibilidade durante todo este percurso e por todas horas despendidas a responder às questões que foram surgindo. Peço desculpa por qualquer cabelo branco ganho à minha custa!

Por fim, mas não menos importante, à minha família e amigos que nunca me deixaram de surpreender com o apoio incondicional que me ofereceram durante todo o este processo. Esse mesmo apoio foi vezes sem conta o "empurrão" que não me deixou desistir dos objetivos inicialmente traçados.

This work was supported by the "Contrato-Programa" UIDB/04050/2020 funded by national funds through the FCT I.P., the Centre of Molecular and Environmental Biology (CBMA) and the STREAMECO project (Biodiversity and ecosystem functioning under climate change: from the gene to the stream, PTDC/CTA-AMB/31245/2017). The work was also supported by CCDR-N (Norte Portugal Regional Coordination and Development Commission) and European Funds (FEDER/POCI/COMPETE2020) through the project AgriFoodXXI (NORTE-01-0145-FEDER-000041)

NORTE-01-0145-FEDER-000041

Development and consolidation of research in the agrifood sector in Northern Portugal

PTDC/CTA-AMB/31245/2017

Cofinanciado por:

STATEMENT OF INTEGRITY

I hereby declare having conducted this academic work with integrity. I confirm that I have not used plagiarism or any form of undue use of information or falsification of results along the process leading to its elaboration.

I further declare that I have fully acknowledged the Code of Ethical Conduct of the University of Minho.

RESUMO

Dados provenientes de deteção remota e observação da Terra são cada vez mais utilizados para a monitorização e avaliação do estado da saúde de ecossistemas bem como das suas funções. Com o desenvolvimento de novas tecnologias, sensores montados em plataformas UAV fornecem dados de deteção remota a resoluções com maior precisão que aquela encontrada em satélites, apesar de não conseguirem cobrir tanta área como estes últimos. A ponderação destes prós e contras dá origem ao problema de correlacionar os dados provenientes de ambas as fontes. Nesta tese são apresentadas uma análise detalhada e uma comparação entre dados multiespectrais de habitats ripários captados em quatro afluentes (CAB1, RAB2, VEZ2 and VEZ3). Com base em dados multiespectrais capturados por um sensor Micasense Rededge™ montado num DJI Phantom 4 RTK e pelos satélites Sentinel-2, foi feita a caracterização dos afluentes utilizando o índice NDVI (*normalized difference vegetation index*). O NDVI foi considerado para este estudo uma vez que a sua relação com o estado de saúde das comunidades de plantas é bem conhecida. As imagens captadas por UAV foram redimensionadas em três processos diferentes para igualar a resolução espacial do satélite (10x10m): média, mediana e terceiro quartil. Para testar qual das imagens redimensionadas se aproximava mais à de satélite, foram usadas medidas de *goodness of fit* (RMSE e R^2). Os resultados demonstram que nas resoluções nativas, os valores de NDVI apresetam o máximo de dispersão, o que é esperado dada a maior divergência na escala das resoluções. O método de *upscale* por terceiro quartil foi o que mais se aproxima aos dados de satélite. Uma segunda análise foi feita para avaliar qual era a maior causa da dispersão de valores dentro do terceiro quartil. Foi encontrada uma maior influência do tipo de uso do solo que na localização dos rios, sendo os campos agrícolas os que apresentam maior discrepância, maioritariamente devido a diferenças no uso do solo (rotação de baldios) e a diferentes estádios de crescimento das colheitas. Este método comparativo devia ser utilizado em diferentes ecossistemas, índices e intervalos temporais para avaliar a sua fiabilidade

Palavas-chave: deteção remota; UAV; Sentinel-2; vegetação ripária; escalamento

ABSTRACT

Remote sensed data is increasingly being used to monitor and evaluate ecosystem health and functions. With the dawn of new technologies, UAV platform mounted sensors provide remote sensing data at spatial resolutions that are far more precise than satellite, however the spatial extent to which a UAV covers is diminutive when compared to that of satellite. This trade-off between pros and cons raises a problem in correlating image data from both sources. In this thesis, a detailed analysis and comparison of riparian habitat multispectral data between UAV and satellite at four different river reaches (CAB1, RAB2, VEZ2 and VEZ3) is presented. Based on multispectral data, captured from a Micasense Rededge™ sensor mounted on a DJI Phantom 4 RTK and Sentinel-2 satellites, the characterization of the stream reaches was possible using the normalized difference vegetation index (NDVI) maps. NDVI was considered due to its well-known relationship to plant community health. UAV images were rescaled to match satellite resolution (10x10m pixel) by three distinct methods: average, median and third quartile. To test which one was closer to satellite values, goodness of fit measures (RMSE and R^2) were considered. Results show that at native resolutions, NDVI values differ the most, as is expected due to the higher divergence of spatial resolution. The method that best fitted the satellite values was upscaling by third quartile. A second analysis was made to evaluate what caused dispersion within the third quartile upscale. Significantly higher influences of land cover type were confirmed when compared to river location, with farmland showing the greatest discrepancy mainly because of differences in farm plot use (fallow rotation) and crop growth stage. This proposed comparative method should be extended to different ecosystems, indices and time frames in future studies to further evaluate his reliability.

Keywords: remote sensing; UAV; Sentinel-2; riparian vegetation; rescaling

TABLE OF CONTENTS

LIST OF FIGURES

LIST OF TABLES

LIST OF SUPPLEMENTARY MATERIAL FIGURES

LIST OF SUPPLEMENTARY MATERIAL TABLES

1. INTRODUCTION

1.1. *Anthropogenic influence in riparian ecosystem functions and services*

As Human growth and expansion move ever onwards, we've become a major threat to ecosystems by changing their processes and functioning, leading to a worldwide decrease in biodiversity (Piégay et *al.*, 2020; Tilman et al., 2012, 2017). Studies (Daily et *al.*, 2000; Loreau et *al.*, 2002) show the changes in biodiversity directly affect the functioning of ecosystems and the goods and services they provide to society. Vitousek et *al.*, (1997) calculated that 30-50 % of the world's land surface has been transformed by human action. Pollution, waste disposal, riparian simplification, bank alteration, straightening and dam construction – human actions increasingly driven by our demands for energy – affect river ecosystems (Bruno et *al.*, 2016; Pievani, 2014; Sabater, 2008). As such, the Anthropocene is of interest for river scientists and fluvial geomorphologists who investigate future changes, management applications and decision-making support (Piégay et *al.*, 2020).

Freshwater ecosystems give crucial functions and services, by providing food, water supplies and water purification, transport of sediments and nutrients, habitats that support biodiversity, create recreational opportunities and enhance the overall quality of human life (Postel & Richter, 2003), and yet, they are deteriorating especially fast due to anthropogenic pressures, being some of the most damaged ecosystems in the biosphere, with some of the highest rates of species loss (Rundle, 2002; Wall et *al.*, 2001).

Riparian zones represent transitional areas occurring between land and freshwater ecosystems, being recognized as areas of biological, physical and chemical interaction and, consequently, are typified by unusually high biodiversity and diversity of environmental processes (Gregory et *al.*, 1991), containing a diverse collection of valuable species and being regarded as biodiversity corridors (Corbacho et *al.*, 2003; Dwire et *al.*, 2018). Riparian vegetation (i.e. plant communities in streams, riverbanks and in floodplains) is present across nearly all riverine domains, and as such, plays a vital role in the health of the ecosystem (Tomsett & Leyland, 2019), (Mligo, 2017). Being diverse in species, structure and regeneration processes (Maingi & Marsh, 2006), riparian plant communities exhibit a high degree of structural and compositional diversity (Gregory et *al.*, 1991), making it extremely difficult to access the current state of biodiversity loss as a result of human disturbance (Oliveira et *al.*, 2004). Fluvial changes are driven by a complex system of drivers, pressures and impacts, one of which is the composition and evolution of the

plant communities that inhabit riparian zones. Climatic change also leads to significant alterations at the physiological level of plants, namely leaf unfolding and flowering of plants in spring or colour changing and leaf fall in autumn (Gordo & Sanz, 2010), as well as an increase in the susceptibility of plant species to pathogens and pests, causing tree die-offs and changes in the distribution of vegetation at a regional level (Bodner & Robles, 2017; Breshears et *al.*, 2005). It is therefore of major importance to monitor these river corridors to understand their processes, characterize evolutionary trajectories, maintain their ecological sustainability and preserve them as a resource for future generations (Piégay et *al.*, 2020), (Tomsett & Leyland, 2019).

1.2. *Remote sensing for monitoring ecosystems*

Earth observation (EO) can be defined as the gathering of information about the physical, chemical, and biological systems of planet Earth. It can be performed via remote-sensing technologies and by ground-based techniques (*International Journal of Applied Earth Observation and Geoinformation ,* 2012). As such, EO is instrumental in for monitoring ecosystems, for it provides information about changes in ecosystems at local, regional, and global scales, being a powerful tool for conservation planning (Vihervaara et *al.*, 2017). Due to the rapid changes occuring throughout Earth's biosphere, quick spatio-temporal assessment is difficult using conventional methods, however, thanks to technological advances, remote sensing platforms now come with higher spatial resolutions (which in turn translates to a decrease in pixel area, and an increase in homogeneity of soil/vegetation cover characteristics inside the pixel), broad coverages and high revisit frequency, which facilitates in the acquisition of data (Bollas et *al.*, 2021; Torresani et *al.*, 2019; Westoby et *al.*, 2012).However, this also raises new challenges in terms of processing and software needs for conservation and biodiversity activities (Corbane et *al.*, 2015; He et *al.*, 2015; Lang et *al.*, 2015; Rocchini et *al.*, 2015).

One of the growing fields in EO techniques in the past decades is remote sensing (from now on referred to as RS). RS can be defined as a range of techniques and methods used to monitor the earth's resources and to acquire information about spatial objects and phenomena without physical contact (usually through platform mounted sensors) (**Fig.1**) (Bollas et *al.*, 2021; Piégay et *al.*, 2020; Pinter et *al.*, 2003). RS uses the electromagnetic spectrum (visible, infrared and microwaves) to extract data from the spectral reflectance characteristics of targets at a distance (Bollas et *al.*, 2021; Shanmugapriya et *al.*, 2019).

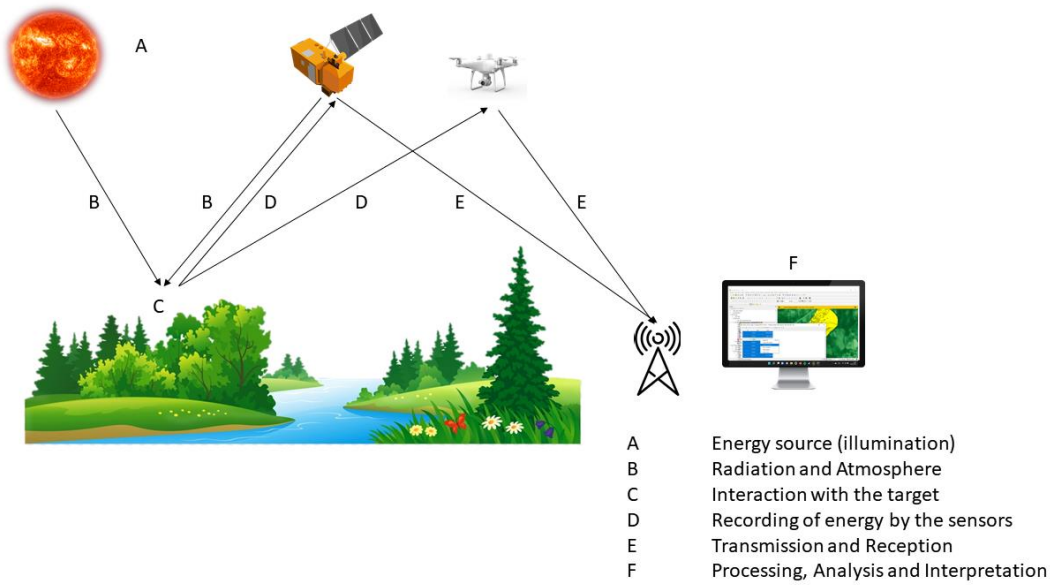

Figure 1. Elements and processes of a remote sensing system (modified from Walton, 1989).

With a growth in multispectral and hyperspectral sensors, RS applications have been employed in different fields, such as crop growth monitoring, land use pattern and land cover changes, mapping of water resources and water status under field condition, monitoring of diseases and pest infestation, forecasting of harvest date and yield estimation, precision farming and weather forecasting purposes along with field observations (Atzberger, 2013; Di Gennaro et *al.*, 2019; Kingra et *al.*, 2016; Messina et *al.*, 2020; Shanmugapriya et *al.*, 2019). RS techniques (along with GIS) have recently been applicable in riparian zones with good results, for they allow the creation of spatio-temporal basic informative layers which can be successfully applied to diverse fields including flood plain mapping, hydrological modelling, surface energy flux, urban development and stress detection (Alleaume et *al.*, 2018; Barton, 2012; He et *al.*, 2015; Kingra et *al.*, 2016; Nezhad et *al.*, 2018; Pinter et *al.*, 2003; Rocchini et *al.*, 2015; Tomsett & Leyland, 2019). The usage of satellites as platforms for remote sensing is not a novelty for the scientific world (Brekke & Solberg, 2005; Holmgren & Thuresson, 1998; Martin, 2008; Tucker & Sellers, 1986; Verbyla, 1995), with studies dating back more than 40 years. Since the launch of the first civilian earth-observing satellite in 1972, satellite remote sensing has provided an ever increasing sophisticated information on the structures and functions of the earth's surface (Iverson et *al.*, 1989), with modern satellites systems like Pléiades 1, KOMPSAT-3 and SuperView-1 offering an impressive resolution of just 0,5m/pxl. Sentinel-2 satellite has been extensively used (Bollas et *al.*, 2021; Cavur et *al.*, 2019; Di Gennaro et *al.*, 2019; Ghoussein et *al.*, 2019; Khaliq et *al.*, 2019; Messina et *al.*, 2020, 2020;

Nezhad et *al.*, 2018, 2019; Pace et *al.*, 2021; Revill et *al.*, 2020; Xu et *al.*, 2021) in different fields of knowledge (conservation, engineering, urban planning, etc) and it is a well-established and powerful remote sensing tool, most of the times chosen based on its decametric resolution in terms of space and time, with a ground sample distance of up to 10m, revisit time of six days, field of view of 290km and a free access dataset that is easily available. Similar to satellite platforms, UAV mounted sensors are being used more and more in scientific studies (Abdullah et *al.*, 2021; Berni et *al.*, 2009; Casado et *al.*, 2015; De Luca et *al.*, 2019; Dubbini et *al.*, 2015; Kislik et *al.*, 2018, 2020; Pontoglio et *al.*, 2021; Themistocleous, 2014) in recent years, mainly because these platforms are becoming increasingly more available and reliable, offering unrivalled spatial resolution over small and medium sized areas and a revisit time that's basically defined by the user (Berni et *al.*, 2009; Klemas, 2015; Piégay et *al.*, 2020; Shanmugapriya et *al.*, 2019). However, both technologies have a series of pros and cons that involve technological, economic and operational factors. UAV platforms come with limitations that hinder wide scale implementation, such as a limited payload and short flight endurance (Matese et *al.*, 2015), while satellite surveys still present coarse resolutions for finer scale classifications, are subject to cloud cover and the fixed-timing acquisitions can, for instance, miss out on specific growth stages of vegetation (Matese et *al.*, 2015). Although there is familiarity with both platforms for ecological purposes, the conjoined use and, most importantly, the comparison of both Sentinel-2 and UAV images is still a very recent endeavour that scientists are trying to understand (Alvarez-Vanhard et *al.*, 2020; Bansod et *al.*, 2017; Bollas et *al.*, 2021; Di Gennaro et *al.*, 2019; Khaliq et *al.*, 2019; Messina et *al.*, 2020; Revill et *al.*, 2020). This comparison of data with different native resolution involves the application of spatial statistics and requires tackling the problem of spatial autocorrelation and although methods are becoming available to compare maps accounting for the spatial structures present in the data, the most practiced procedures still rely on cell-by-cell evaluations (Matese et *al.*, 2015).

It's also important to note that, even though UAV and satellite studies are being more commonplace (as shown above), studies using comparisons of both platforms in a riparian setting are still scarce (Gómez-Sapiens et *al.*, 2021; Huylenbroeck et *al.*, 2020).

1.3. *Vegetation spectral indices*

Multispectral reflectance of the canopies is related to two important plant physiological processes (photosynthesis and evapotranspiration) (Kingra et *al.*, 2016). Several studies (Asner, 1998; Ceccato et *al.*, 2001; Datt, 1998; Gupta et *al.*, 2003; Pu et *al.*, 2003; Stimson et *al.*, 2005)

focused on the spectral reflectance properties of the plants, identifying key spectral wavebands related to plant physiological and structural properties and from there, derived vegetation spectral indices for their non-destructive estimation. The potential to spectrally estimate plant physiological properties over relatively large areas, and to predict plant water status and plant water stress has already been demonstrated in forestry species (Stimson et *al.*, 2005). RS data has been used to estimate canopy characteristics by using spectral indices based approach (D'Urso et *al.*, 2004). Chlorophyll pigments absorb radiation in the blue and red part of the electromagnetic spectrum and reflects in the green; nevertheless, the percentage of radiation reflected from the leaf is higher in the NIR than in the green (Chappelle et *al.*, 1992; Gausman et *al.*, 1971). The spectral reflectance of the leaf in healthy plants is characterized by high values of reflectance in the NIR region and low values in red portion (absorption) (Pinter et *al.*, 2003), while the opposite behaviour (more red light reflectance and more absorption in NIR) can be expected in plants subjected to stress.

Numerous spectral vegetation indices (VIs) have been developed to characterize vegetation (Kingra et *al.*, 2016), but for the sake of this investigation, we shall only mention the Normalized Difference Vegetation Index (NDVI) proposed by Rouse et *al.*, (1973), as this was the method implemented in the experiment. NDVI has become a commonly used vegetation index to assess vegetation condition (Barton, 2012; Wallace et *al.*, 2004) for it allows to measure the state of the vegetation based on how it reflects light at certain frequencies. It's designed to evidence photosynthetic activity from a surface, taking advantage of the strong contrast in vegetation reflectance observed between the red spectral and NIR spectral domain (Alleaume et *al.*, 2018). However, it has to be taken into account that the validity of NDVI values are influenced by many factors, such as: surface properties, anisotropic effects (position of the sun and observer) and atmospheric conditions (Alleaume et *al.*, 2018).

1.4. *Study Objectives and Hypothesis*

With all these facts in mind, the main objectives for this study are:

1) Evaluate the accuracy of satellite data by comparing to UAV data;

2) Evaluate which rescale methods assure best fitness among drones and satellite;

3) Evaluate the influence of land cover on the discrepancy among drone and satellite data.

Native data source is expected to have higher dispersion from corrected (rescaled) data since there's a bigger difference in pixel area from both platforms.

Higher dispersion in NDVI is also expected in natural land cover compared to anthropogenic land cover. Considering that NDVI is a vegetation index (meaning higher values for green vegetation), the lowest NDVI values are expected to belong to anthropogenic land cover, regardless the platforms used. In addition, it is expected that discrepancies (dispersion of data) in NDVI values for man-made buildings will be the lowest and not influenced by the spatial scale. On the other hand, it's expected that the higher NDVI values will be found in natural land cover. However, in this case, it is also expected a major miss match between platforms due to the heterogeneity of forest and bush vegetation (i.e the presence of riparian trees, shrubs and mixed vegetation can be spatial scale dependent) is also predictable.

2. MATERIALS AND METHODS

2.1. *Study sites*

Four stream reaches in two river basins across the Northwest of Portugal were selected: the Lima and the Cávado River basins, draining to the Atlantic Ocean (**Fig. 2**).

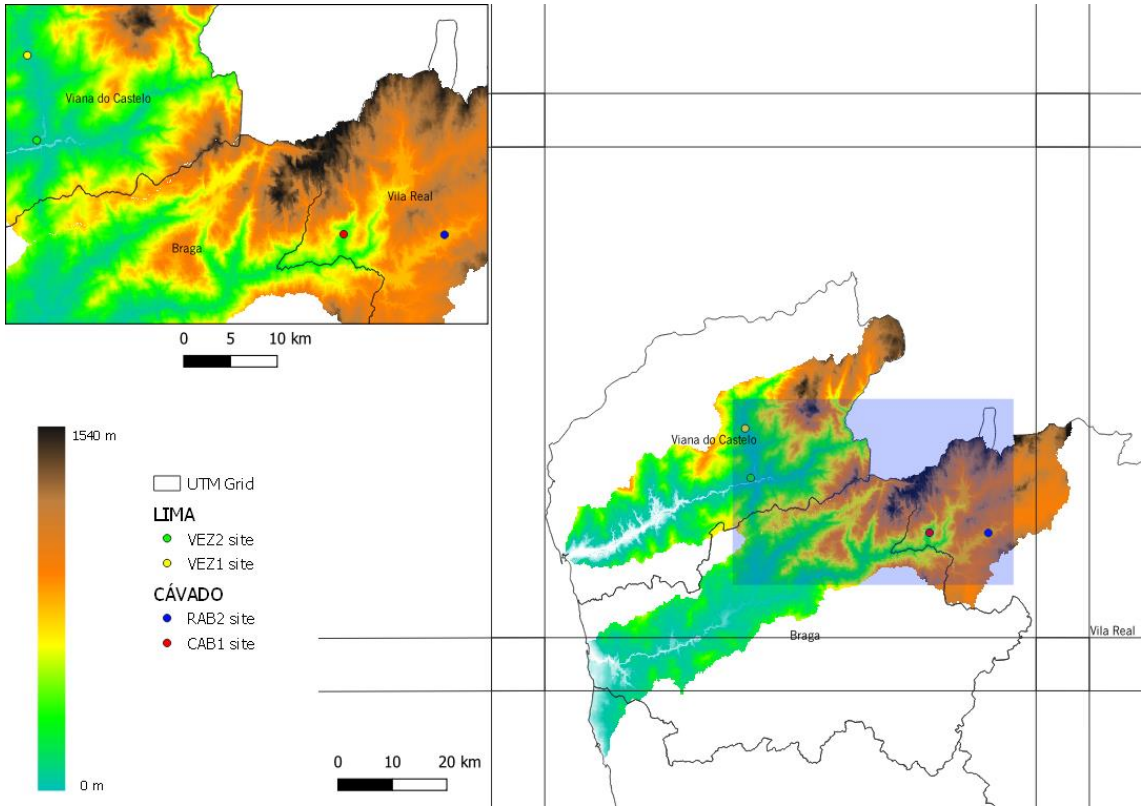

Figure 2. Catchment site's location within NW Portugal.

4 study sites within the study area were chosen for UAV image capturing: Ribeira de Cabril, Rabagão and two sites in Rio Vez (**Fig. 3**).

The sites were chosen based on the location of the flights previous to this study. Vez had two different sites (one before and other after the village of Arcos de Valdevez), as one of the original objectives was to evaluate the influence of human settlements in riparian ecosystem health. Although this objective was later abandoned, the sites chosen remained the same.

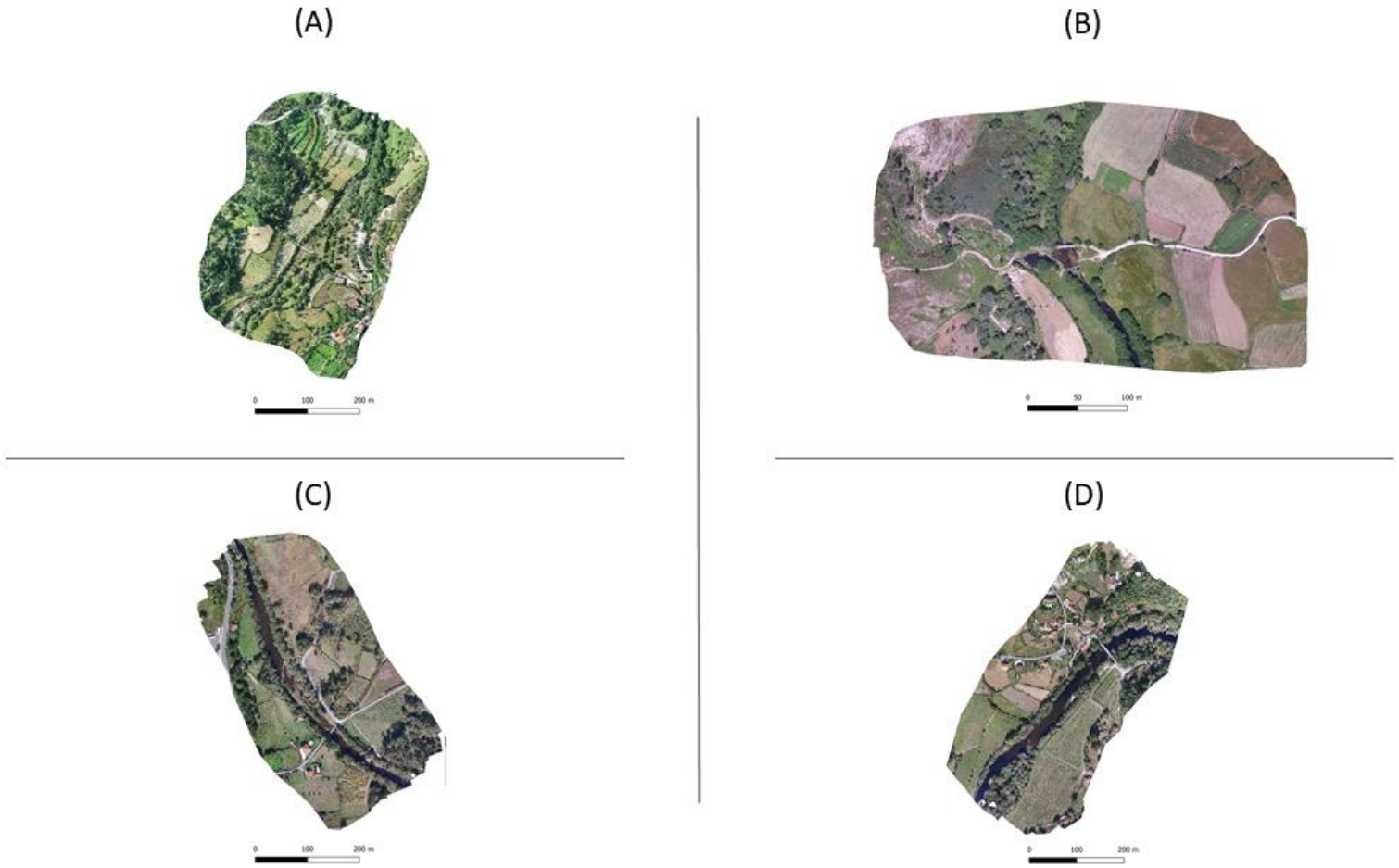

Figure 3. UAV orthophotos of study sites. (A), (B), (C) and (D) refer to Ribeira do Cabril, Rabagão and Rio Vez, respectively. (see ANNEX I)

In a general way, all sites are characterized by a corridor of riparian vegetation immediately adjacent to the river, with either one or both margins occupied mainly by small plots of farmland and variable areas with grass and bush vegetation cover. Manmade structures such as houses, sheds and barns are present in all sites, with most of the buildings having road accesses from main roadways.

Study sites were named based on the tributary where the images were captured (**Table 1**) and from this point forward they will be addressed by their respective code.

Table 1. Catchment sites specifications and coordinates.

Code	Stream name	River Basin	Latitude	Longitude
CAB1	Ribeira de Cabril	Cávado	41.721487	-8.032822
RAB2	Rabagão	Cávado	41.71956	-7.903389
VEZ2	Rio Vez	Lima	41.896635	-8.438900
VEZ3	Rio Vez	Lima	41.815080	-8.426453

2.2. *Materials and Methods*

2.2.1. *UAV-Based Imagery*

UAV image acquisition took place at 3 different dates: the 10th of July 2018, the 5th of August 2019 and the 11th of October 2019. The chosen images were randomly picked from a database of UAV flights made for the CLIMALERT initiative before the investigation.

Spatial resolution of captured UAV images is 0.08 m at ground level (**Fig. 3**). The multispectral sensor consists of five spectral cameras collecting blue, green, red, red edge and near infrared (NIR) imagery (**Table 2**).

The duration of each flight was approximately 5-10 min, and the images were collected between 10:45 and 12:00, in clear sky conditions for all rivers. Flights were carried out at 100 m height from starting point. Mapping took part with an average overlap 80% forward and sideways. In flight triggers were: 233 at CAB1; 287 at RAB2; 351 at VEZ2; 409 at VEZ3.

Table 2. Bands and their wavelengths for both Sentinel-2 (adapted from Bertini et *al.*, 2012) and Micasense Rededge™ (RedEdge User Manual (PDF)) camera mounted on the DJI Phantom 4 RTK.

Sensing Platform	**Band Number**	**Band**	**Central Wavelength (nm)**	**Bandwidth (nm)**	**Spatial Resolution (m)**
Sentinel -2	1	Violet	443	20	60

	2	Blue	490	65	10
	3	Green	560	35	10
	4	Red	665	30	10
	5	Rededge	705	15	20
	6	Near Infrared	740	15	20
	7		783	20	20
	8		842	115	10
	8b		865	20	20
	9		945	20	60
	10		1380	30	60
	11	Short Wavelength Infrared	1610	90	20
	12		2190	180	20
Micasense Rededge™	1	Blue	475	20	0.08
	2	Green	560	20	
	3	Red	668	10	
	4	Near Infrared	840	40	
	5	Rededge	717	10	

2.2.2. *Satellite time series imagery*

The Sentinel-2 mission is a two satellite (Sentinel-2A and Sentinel-2B) constellation launched by the Copernicus European Program for Earth observation, providing high-resolution, multispectral images (European Space Agency, 2015). The captured data of Sentinel-2 ranges from the visible to the shortwave infrared parts of the electromagnetic spectrum with 13 spectral bands at 3 different spatial resolutions. Satellite data was downloaded via https://scihub.copernicus.eu (accessed on 5 June 2021) from both the S2A (CAB1 and RAB1) and S2B (VEZ2 and VEZ3) satellites with the spatial resolution of 10 m at ground level. All acquired images are located within the 29TNG tile (UTM tiling grid) from a Level-2A product (atmospherically corrected). Images for RAB2 are from 9 July 2018 at 14:23:05 UTC (10.59% cloud cover), for CAB1 from 3 August 2019 at 14:18:08 UTC (0.89% cloud cover) and for both VEZ2 and VEZ3 from 10 October 2019 at 14:13:58 UTC (0.17% cloud cover) and the images were chosen based on the temporal proximity (1-2 days) to the previously made UAV flight dates to allow for a more viable correlation between the data, as temporal differences account for different stages of vegetation growth, and as such, different NDVI values.

2.3. *Earth observation data*

For this study, all image post-processing was done using QGIS v3.16.15 “Hannover” (long term release) software. UAV orthophotos (**Fig 4**) were used to classify land cover in all sites for

they allow by far the best perception of the study site, enabling a more trustworthy description and classification of land cover. Classification was achieved by manually "drawing" each different polygon and labelling them accordingly. The reason for manually doing this instead of using an object-based machine learning image classification software was that most of the software's tried and easily available didn't have enough precision to correctly classify different land covers at the scale of the UAV images (some polygons have areas of $<0.2m^2$). 7 distinct categories were attributed to the polygons based on their different characteristics: River; Road; Bush Vegetation; Forest Vegetation; Grass; Farm; Man Made Structure (see **ANNEX IV**).

2.4. *Normalized Difference Vegetation Index*

The normalized difference vegetation index (NDVI) as proposed by Rouse et *al.*, (1973) was designed to evidence photosynthetic activity from a surface, taking advantage of the strong contrast in vegetation reflectance observed between the red spectral and NIR spectral domain.

Taking only into account these two spectral bands, NDVI is calculated as seen bellow in **Equation 1**:

$$NDVI = \frac{NIR\text{-}RED}{NIR+RED} \quad (1)$$

where NIR stands for near infrared band reflectance and RED for the red band reflectance (see **Table 2** for more information regarding the bands).

2.5. *Data processing and analysis*

A well-defined step-by-step process was created for the conduction of data processing and analysis to achieve all goals of the study (**Fig. 5**).

All images were registered to CRS WGS84/UTM zone 29N with EPSG:32629. NDVI maps were obtained using the **Equation 1** in the "Raster Calculator" tool using the respective NIR and Red bands for each platform (**Fig. 6**).

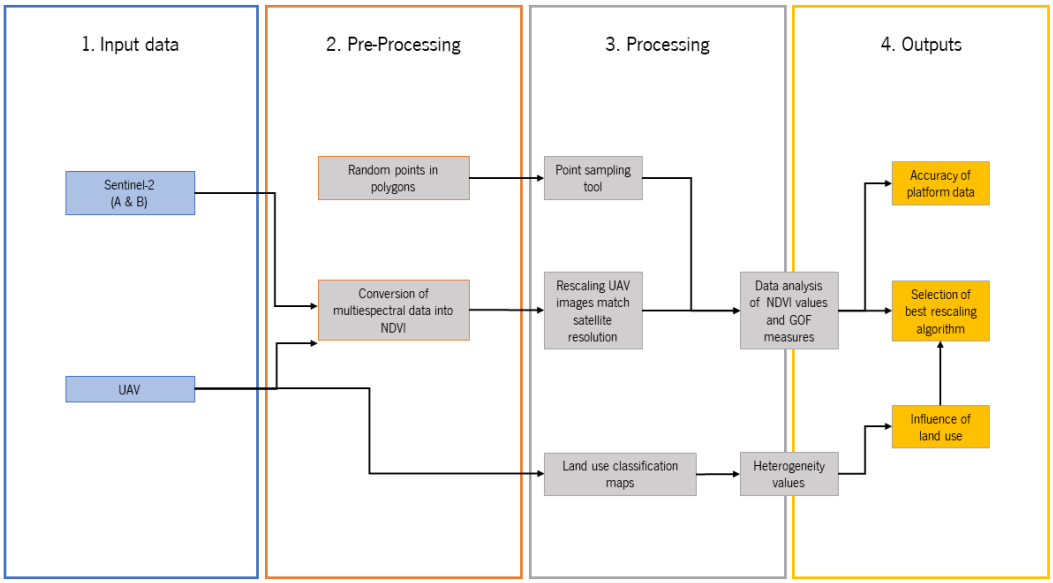

Figure 4. Flow chart of the proposed methodology for data processing and analysis used in the current study.

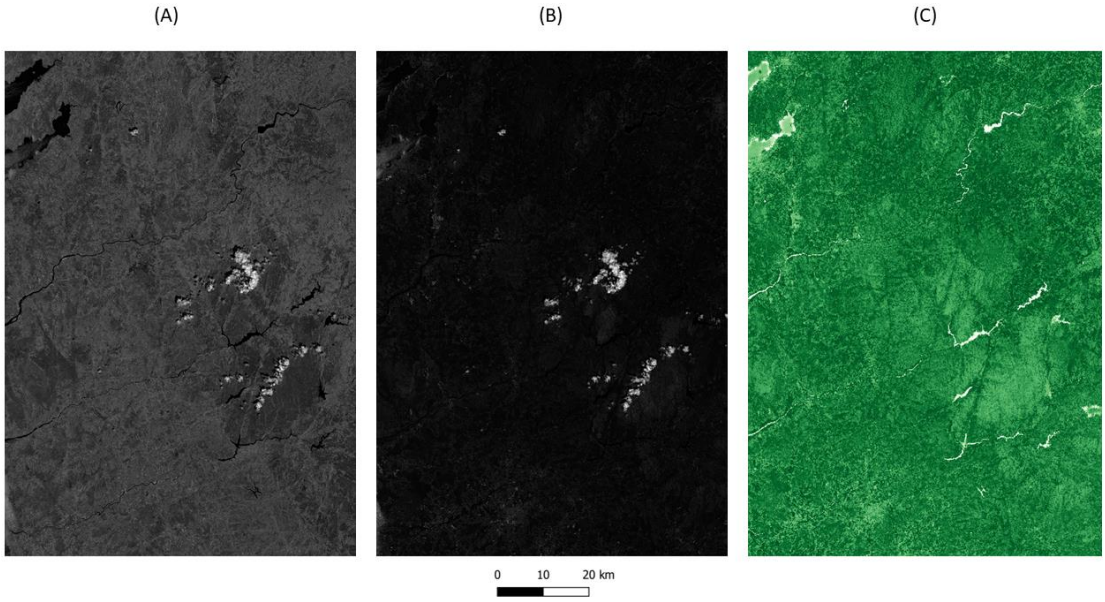

Figure 5. Example of raw and processed satellite images from 09/07/2018 directly downloaded from source. NIR and Red band can be seen in (A) and (B) respectively and the calculated NDVI resulting layer (C).

2.5.1. *Data processing*

UAV images where rescaled to match the spatial resolution of the satellite imagery (10 m) using the "Raster Warp" built-in tool directly on the NDVI layer at native resolution (0.08 m) (**Fig. 15**).

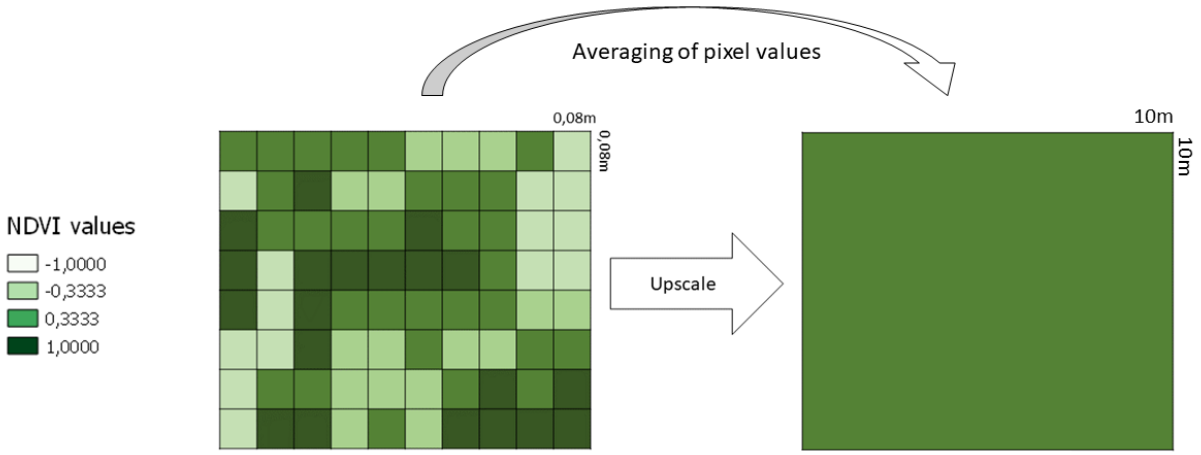

Figure 6. Example of information loss from the averaging process in the upscaling method.

3 of the 12 rescaling methods in QGIS, were chosen based on their apparent proximity to the satellite image, the following being: average, third quartile and median. For the sake of brevity, from now on, these rescaling methods shall be addressed to as AV (average), 3Q (third quartile) and MN (median).

A set of 5000 random points was generated for each site using the "Random Points in Polygon" vector research tool. These same points are used to retrieve both the NDVI values from UAV and satellite images and the type of land cover at which point is located. This is attained by using the "Point Sampling Tool" (v 0.5.3) plugin. Datasets generated were exported in text format with integer values.

2.5.2. *Data analysis*

First, in order to evaluate discrepancies among NDVI values from satellite with NDVI from UAV platform, linear regression models (lm command in Rstudio) were applied. Statistical assumptions were previously tested before application of linear models. 4 models were tested using the native resolution and the three rescaled algorithms (AV, 3Q and MN). The dataset used in this analysis has the entirety of sampling points (n = 75544).

Second step was to attribute features relative to land cover categories and river reach to each sampling point based on land cover maps (see **ANNEX IV**). Next step was to test new linear regression models considering land cover and river reach variables associated to each sampling point (**Equation 3, 4 ,5 and 6**).

$$Linear\ Regression\ Model = lm\ (NDVI_{Native} \sim NDVI_{Satellite} + Land\ use + River\ Reach) \quad (3)$$

$$Linear\ Regression\ Model = lm\ (NDVI_{AV} \sim NDVI_{Satellite} + Land\ use + River\ Reach) \quad (4)$$

$$Linear\ Regression\ Model = lm\ \left(NDVI_{3Q} \sim NDVI_{Satellite} + Land\ use + River\ Reach\right) \quad (5)$$

$$Linear\ Regression\ Model = lm\ (NDVI_{MN} \sim NDVI_{Satellite} + Land\ use + River\ Reach) \quad (6)$$

This way we can assess the influence of land cover on the discrepancy among drone and satellite data.

In addition to this, 2 out of 20 Goodness-of-fit (GOF) measures were considered for different purposes – in order to find the best fit model we used RMSE and to evaluate dispersion of values within methods we used R^2. These metrics can be calculated by **Equations 7 - 8**. RMSE and R^2 were chosen based on their extensive use in remote sensing studies (Cai et *al.*, 2018; Han et *al.*, 2018; ten Harkel et *al.*, 2019; van der Meij et *al.*, 2017), reliability and capability to both assess how the regression models fit the datasets and quantify the proportion of the variance in the response variable that can be explained by the predictor variable.

$$RMSE = \frac{\sqrt{\sum(Pi-Oi)^2}}{n} \quad (7)$$

where Pi is the predicted value for the i^{th} observation in the dataset and O_i is the observed value for the i^{th} observation in the dataset

$$R^2 = \frac{TSS-RSS}{TSS} \quad (8)$$

where TSS is the Total Sum of Squares and RSS is the Residual Sum of Squares.

All data analysis in this study was performed in Rstudio (v1.4) with the aid of ggplot2 and HydroGof (v 0.4) packages.

3. RESULTS

3.1. *Evaluating discrepancies between satellite and UAV images.*

The results for linear regression models between satellite NDVI data with UAV, at native and rescaled resolutions, data is reported in **Table 3** and **Fig. 8**.

Significant relationships (p-value = < 2E-16) were found in rescaled and native resolutions of data. However, R^2 values varied among linear models. The model based on native data presented the lower R^2 (R^2_{native}= 0.2397), whereas the highest values were found for the Average rescaled algorithms (R^2_{AV}= 0.4228). High dispersion of data was found when total NDVI values between satellite and UAV, at native and rescaled resolutions, were compared (See **ANNEX VII**).

Table 3. Results of linear regression models applied to total NDVI data of different rescaled methods.

	Native			3Q			AV			Median		
	Estimate	Std. Error	t value	Estimate	Std. Error	t value	Estimate	Std. Error	t value	Estimate	Std. Error	t value
intercept	0.050	0.006	8.525	0.178	0.004	46.04	0.069	0.004	18.94	0.046	0.005	9.403
ndvi_sat	0.648	0.008	77.158	0.601	0.006	108.21	0.619	0.005	117.6	0.662	0.007	94.131
R^2	0.2397			0.3827			0.4228			0.3199		
p value	< 2.2e-16			< 2.2e-16			< 2.2e-16			< 2.2e-16		

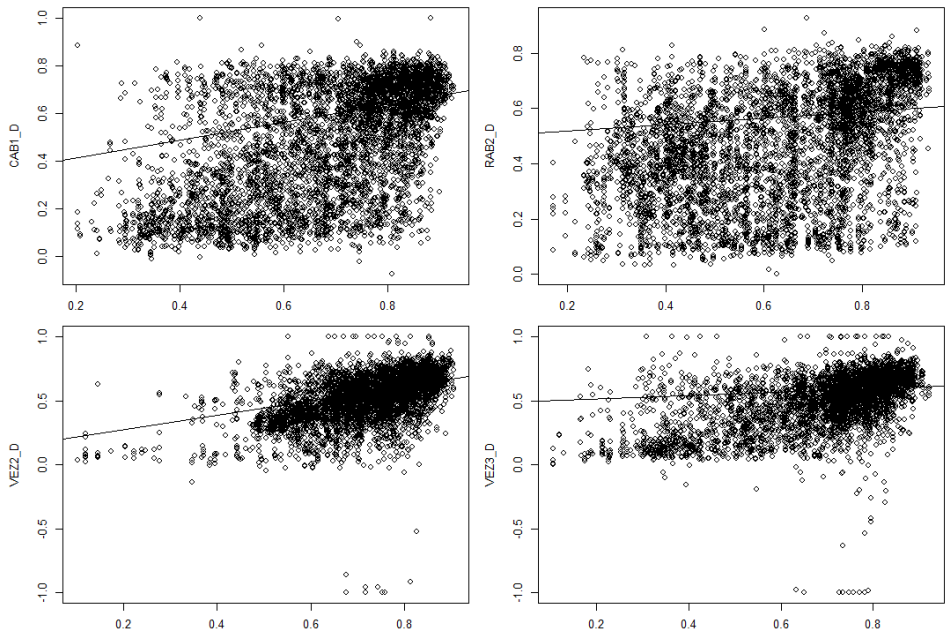

Figure 7. Comparison between UAV and satellite NDVI values at native resolutions for all catchment sites.

3.2. *Influence of land cover*

Land cover maps for each river were reported in **ANNEX IV**. 7 land cover categories were identified: Forest vegetation, bush vegetation, grass, farm, road, river and manmade structures.

By using the classified land cover maps (**Fig. 9**) in conjunction with point sampling tool, random points for data extraction gained land cover and river reach values based on their location (**Fig. 16**). Forest vegetation has less than half area coverage in RAB2 than the rest of the rivers. The same situation is verified with man-made structures, road and river. This can be partially explained, in part, by RAB2 being the catchment site with the smallest area, about 44,5% smaller than VEZ3 which is the largest, associated with the fact that all riparian zones in this study are scarcely populated, with most houses being isolated.

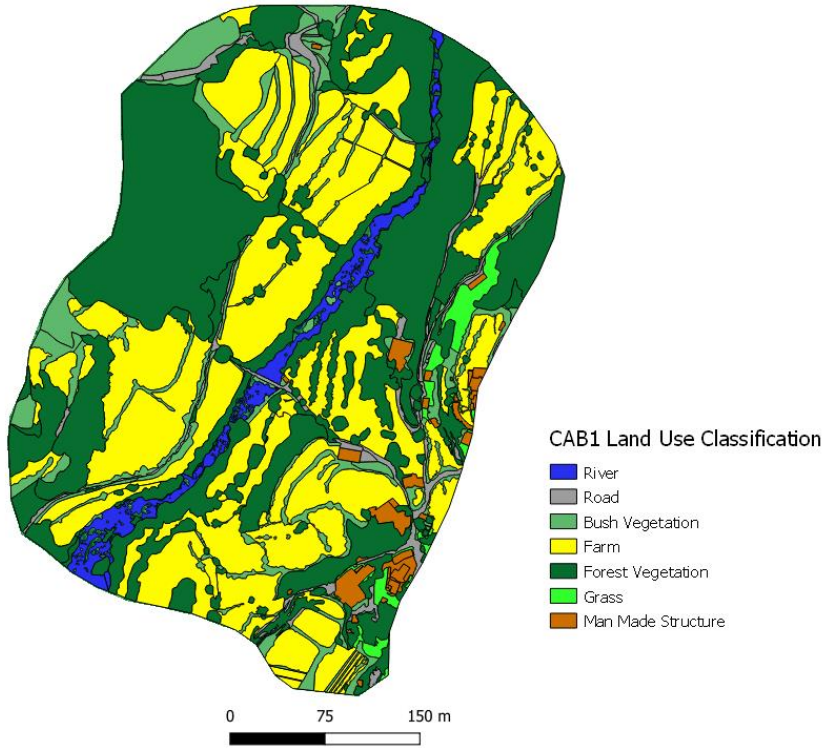

Figure 8. CAB1 site land cover classification map (the rest of the land cover classifications can be consulted in appendix).

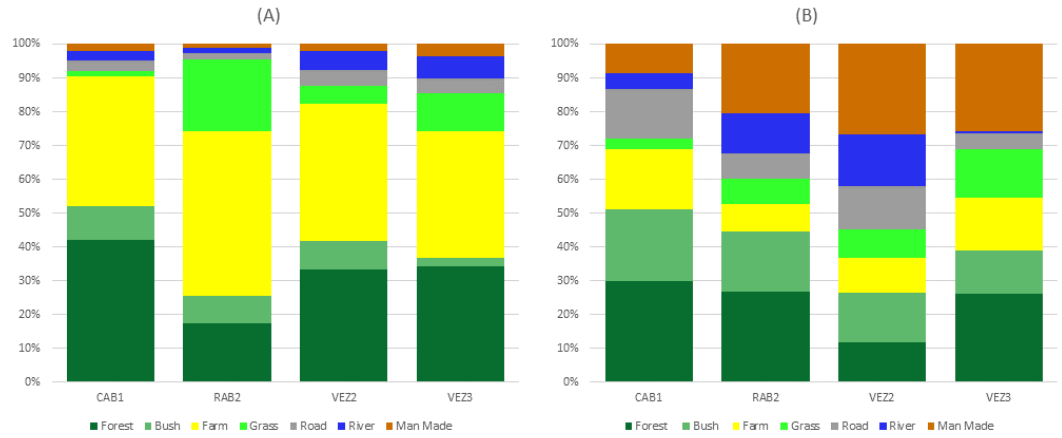

Figure 9. Composition (%) for each land cover classification by (A) area and (B) number of polygons. (see in **ANNEX VI)**

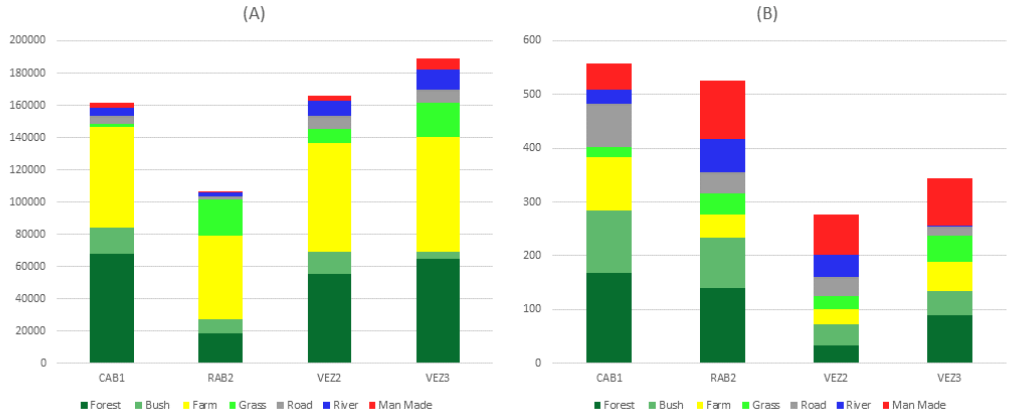

Figure 10. Composition for each land cover classification by (A) area (m2) and (B) number of polygons.

Results on linear regression including land cover and river as predictor variables are reported in **ANNEX VI**. **Table 4** shows an example of the output for the Av algorithm model that resulted with the highest R^2 ($R^2 = 0.483$).

Table 4. Results of linear regression model applied to AV algorithm.

	Estimate	Std. Error	t value
Intercept	0.122	0.005	24.271
ndvi_sat	0.528	0.006	92.155
RAB2	0.038	0.002	16.117
VEZ2	0.027	0.002	11.919
VEZ3	0.0215	0.002	8.975
Farm	-0.028	0.003	-8.645
Forest	0.041	0.003	12.452
Grass	-0.042	0.004	-10.511
Manmade	-0.1	0.006	-15.608
River	-0.098	0.005	-20.322
Road	-0.065	0.006	-6.016
R2	0.483		
p value	< 2.2e-16		

Like previous linear regression models applied to total NDVI values, significant relationships (p-value = < 2E-16) were found among all linear regression models applied this time. This tells us that land cover and catchment site are significant parameters in influencing the dispersion of values within upscaling algorithms. GOF measures for 3Q model showing the lowest RMSE (RMSE = 0.12) are reported in **Table 5** and **Fig. 12**.

Highest value of RMSE (RMSE = 0.510) is seen in native resolution while the lowest in seen in 3Q rescale algorithm (RMSE= 0.12). Average and median rescaled algorithms show similar RMSE values with median $_{Average}$=0.225 and median $_{Median}$=0.235. In contrast, R^2 had the lowest value in native resolution (R^2 = 0.00) and the highest in average upscaling method (R^2 = 0.670).

Table 5. Calculated GOF values for 3Q algorithm.

LandUse	River	RMSE	R2
Forest	CAB1	0.12	0.21
	RAB2	0.14	0.26
	VEZ2	0.14	0.14
	VEZ3	0.14	0.27
Bush	CAB1	0.15	0.28
	RAB2	0.16	0.15
	VEZ2	0.13	0.28
	VEZ3	0.12	0.32
Farm	CAB1	0.18	0.53
	RAB2	0.24	0.01

	VEZ2	0.14	0.59
	VEZ3	0.15	0.54
Road	CAB1	0.16	0.39
	RAB2	0.16	0.17
	VEZ2	0.18	0.28
	VEZ3	0.16	0.39
Man	CAB1	0.25	0.1
	RAB2	0.15	0.3
	VEZ2	0.17	0.54
	VEZ3	0.18	0.36
River	CAB1	0.2	0.16
	RAB2	0.16	0.36
	VEZ2	0.21	0.06
	VEZ3	0.29	0.07
Grass	CAB1	0.17	0.1
	RAB2	0.12	0.61
	VEZ2	0.14	0.26
	VEZ3	0.17	0.28

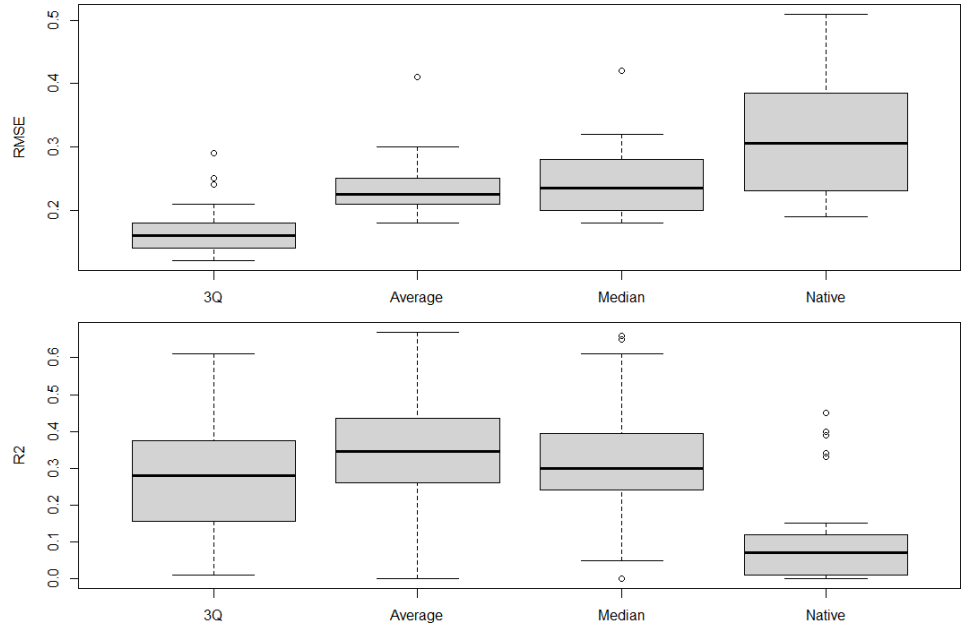

Figure 11. Boxplot of GOF measures resulting from linear regression model to evaluate best fit of rescale to satellite values.

Data subsets containing the GOF values of land cover and type within each different method were created to assess the cause of discrepancy within methods (**Fig. 13**).

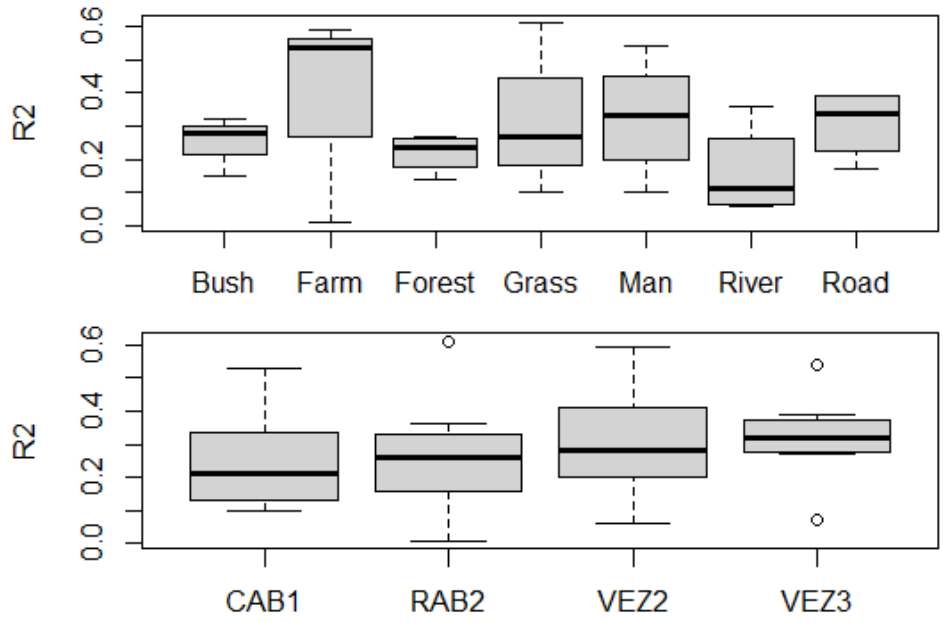

Figure 12. Boxplot representation of linear regression applied to 3Q algorithm subset of GOF measures within a rescaling method.

In **Fig. 14** the relationship between Satellite NDVI with UAV NDVI for 3Q Algorithms. Different trend lines are present for each category of land cover.

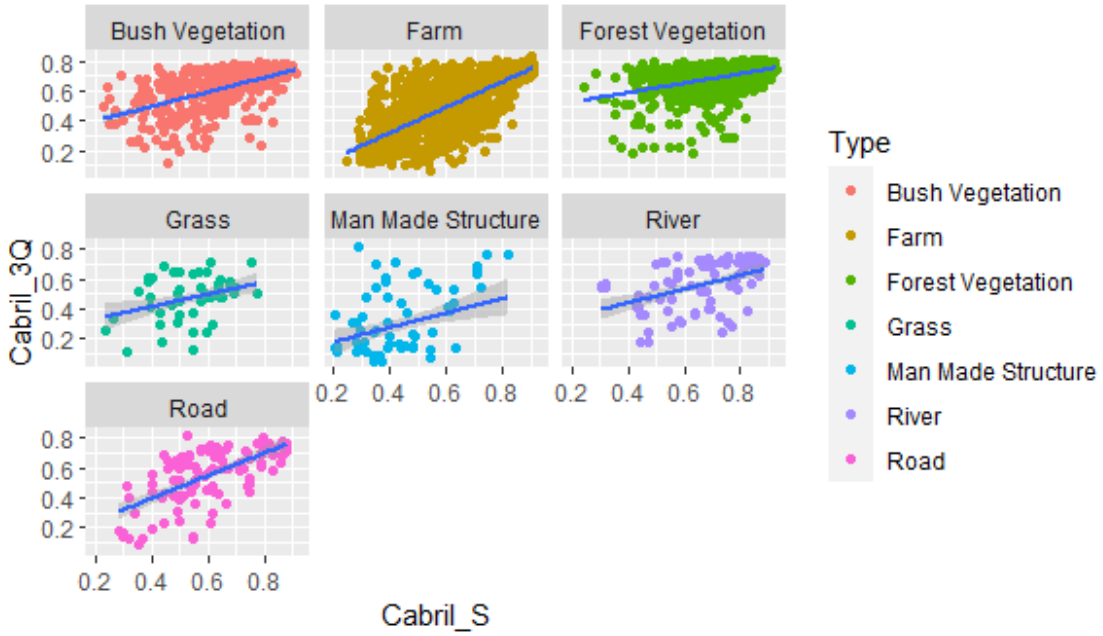

Figure 13. Facet_wrap plot for CAB1. (see **ANNEX VII**)

4. DISCUSSION

4.1. *Comparing NDVI values from UAV and Satellite*

An expected higher degree of dispersion between native resolutions was confirmed, with CAB1 and RAB2 showing the strongest dispersion values of the 4 sites. This is because the biggest discrepancy between pixel area is at native level. While higher NDVI values follow a similar trend both in satellite and UAV (between 0.5 and 1) at native resolution, lower values are much more present in UAV native image capturing. This can be explained by the much higher resolution of the UAV being able to capture more pixels with low values over the same area as satellite.

When comparing rescaling methods, NDVI values show less dispersion, but at the same time, because of the loss of information associated with upscaling process (**Fig. 7**) (Messina et *al.*, 2020) the homogenization of values is high, especially at lower values. A trend (peak) in higher NDVI values can be seen in every rescale. The same peak is present in satellite image histograms for values between 0,5 and 1 (see **ANNEX V**).

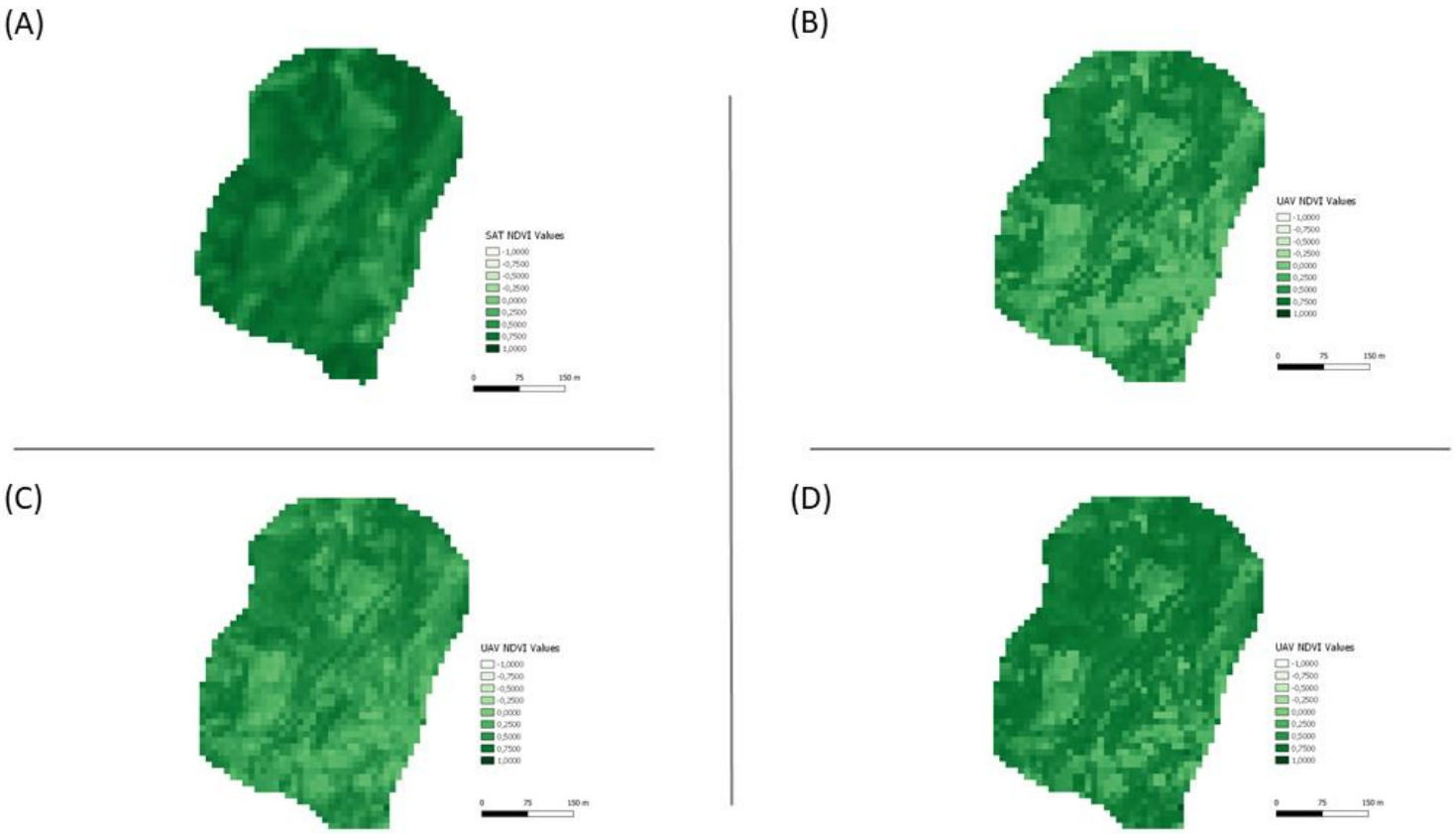

Figure 14. CAB1 NDVI satellite image (A) and UAV rescaled images derived from "Raster Warp" processing of the native resolution. (B), (C) and (D) correspond to the median, average and third quartile rescaling methods, respectively.

4.2. *Finding the best rescaling method and influence factors.*

The proposal for "best method" is based on the one that differs less from the satellite image NDVI values, in other words, the one which produces less error during the upscaling process. Because RMSE measures how far apart the predicted values are from the observed values in a dataset, the choice for best rescaling method was based upon the RMSE values present at **Table 5** and **Fig. 12**. It was concluded that out of the three methods, upscaling via third quartile (3Q) had the best fit with satellite values (RMSE median values (0,16); p-values < 2e-16).

By creating a subset of GOF measures by land cover and river within the best method (3Q) we can find an explanation for dispersion within the group. R^2 is used to measure how statistically similar values in the two datasets are (using a simple linear regression model). This explains the variation within the model or in other words, how land cover or river site affects these values. As confirmed in **Fig. 13**, river sites have very similar median R^2 values, which means they all contribute with about the same level to the dispersion of values, hence, it's concluded they're not the main reason for value differences. On the contrary, by examining land cover, it is evident that there are big differences between R^2 values. **Fig. 13** accounts for catchment site in the land cover values, so what we see is the total R^2 for that land cover within all rivers. Greatest disparity is confirmed in Farm, and by cross referencing this data with a clustered column chart of GOF measures in the subset (see **ANNEX VIII**) we can see that the lowest value comes from RAB2. Revisiting the map in QGIS (**Fig. 16**) gives insight regarding the lowest R^2 value (0.01). RAB2 has the whole east margin covered in farmland. Although there was no *in situ* validation to check if farms were monoculture, at the time the images were captured, some fields were uncultivated, as fallow ground is still widely used in agriculture during crop rotation (Collins et *al.*, 1992) and/or presented different growth stages. Low overall average R^2 (0.22) for "Forest Vegetation" can be associated with different plants that make up the riparian forest community, as different species tend to have different NDVI values. "Forest Vegetation" polygons were drawn based on the tree canopies visible by the UAV orthophotos, ignoring bushes and grasses that make up the entire forest *per se*, which in turn, have different NDVI values than those of the tree canopies. These NDVI values can give us a very coarse idea of plant species richness (Fairbanks & McGwire, 2004), but because there was no ground validation for the study, further research is needed to validate. Lowest overall R^2 belongs to the land class River, probably because the thin and very shallow water column of the analysed streams allowed satellite and UAV to capture NDVI values from river substrate,

algae and macrophytes. Although not accounted for during land classification, algae and macrophytes communities do exist in these rivers (Dodkins et *al.*, 2012; Ribeiro & Torgo, 2008) and account for different NDVI values.

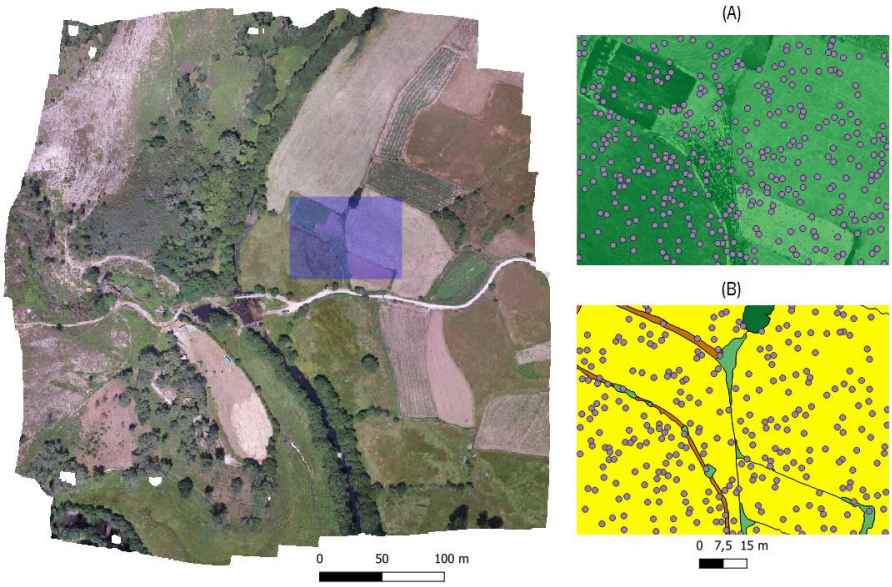

Figure 15. RAB2 farmland examination where (A) is the NDVI map with correspondent randomised points and (B) is the division of land cover with the same points.

4.3. *Land cover and Heterogeneity*

The highest value accounted for % of area coverage in all sites was that of farmland in RAB2 with almost half the map (48,55%), while in the same site we get the lowest value of all, with just 0,98% coverage by manmade structures. On average, throughout all sites, farmland is the type of land cover with more % of area covered, with an average of 41,32 and following the same order, manmade structures only account for 2,12% of total area coverage. Regarding the number of polygons, forest vegetation shows the greater number of polygons per map in CAB1 with 167 polygons of the class present (or 29,98% of the map) being, at the same time, the most polygon rich class across all sites, with 23,58% (or 107,25) of total polygons. On the low end is river polygons with 8,02% (32,75) polygon coverage over all sites, and with the lowest value of all in VEZ3 with only 2 polygons to account for the entire river sections (see **ANNEX IX**).

5. CONCLUSIONS AND FUTURE PERSPECTIVES

The ecological importance of this thesis resides in the ability to correlate satellite and UAV imagery, hence, being able to get the best of both methods in conservation efforts regarding plant community health in riparian zones.

In this study, a detailed analysis and comparison of multispectral imagery of riparian zones in NW Portugal, is presented with the aim to calculate NDVI disparity between both methods, at native as well as rescaled (for UAV) resolutions and based on these results find the upscale method that is closer to satellite imagery. Statistical comparison between NDVI values at native resolution show, as expected, a bigger difference in values than those found in UAV upscaled version, due to the higher spatial resolution of the UAV's sensor.

Upscaling via third quartile seems to be the closest rescale method to satellite (RMSE < 0.2) when it comes to measuring NDVI values in riparian zones with similar characteristics than those in this study. However, we concluded that homogenization of values tends to be highest at lower NDVI values, because UAV image upscaling tends to attribute smaller pixel value than those found in satellite images, which can contribute to reading errors.

Land cover was proven to be the main factor influencing value dispersion within each method, primarily caused by farmland, most of which, at the time of image capturing, had a mix of fallow and cultivated and/or different crop growth stages. Further studies within a time frame that represents a full vegetative season should be considered to greatly reduce or even eliminate this error. Forest and bush vegetation data should also be complemented in further studies with ground validation, for a more accurate classification of riparian ecosystems.

In conclusion, both platforms provide important information for the vegetation cover and land cover on riparian zones, and they are proven again to be important tools for conservation work. The choice for the most appropriate platform depends mainly on the use and the aim of the intended data, as they have different spatial resolutions, cost, and requirements. Sentinel-2 is a valuable platform when information for areas of large extent is needed and therefore is not the optimal method to evaluate ecosystems as complex as riparian zones or as spatially small as the farms of the chosen sites, as these farms resource to farming practices which are typical of this region of Portugal (small, highly fragmented plots of cultivated land, usually with a mix of crops in a small area). As such, UAV platforms are a better choice when detailed information is required.

The lack of studies on the comparison of multispectral data retrieved between Sentinel-2 and UAV imagery was what motivated the explorative approach taken in the present work. Most of

the times it proved to be an obstacle, since no term of comparison and further discussion could be traced between the results found here and the ones described in the literature.

As remote sensing techniques are gradually picking up the pace to become the standard method for evaluation of ecosystem health throughout the globe. Although further studies and techniques in correlating data between UAV and satellite need to be developed, this study demonstrated the potential for the comparison of multispectral data to interpret riparian zone ecosystems.

SUPPLEMENTARY MATERIAL

ANNEX I – Orthophotos of study sites

Figure I A. CAB1 stream reach orthophoto.

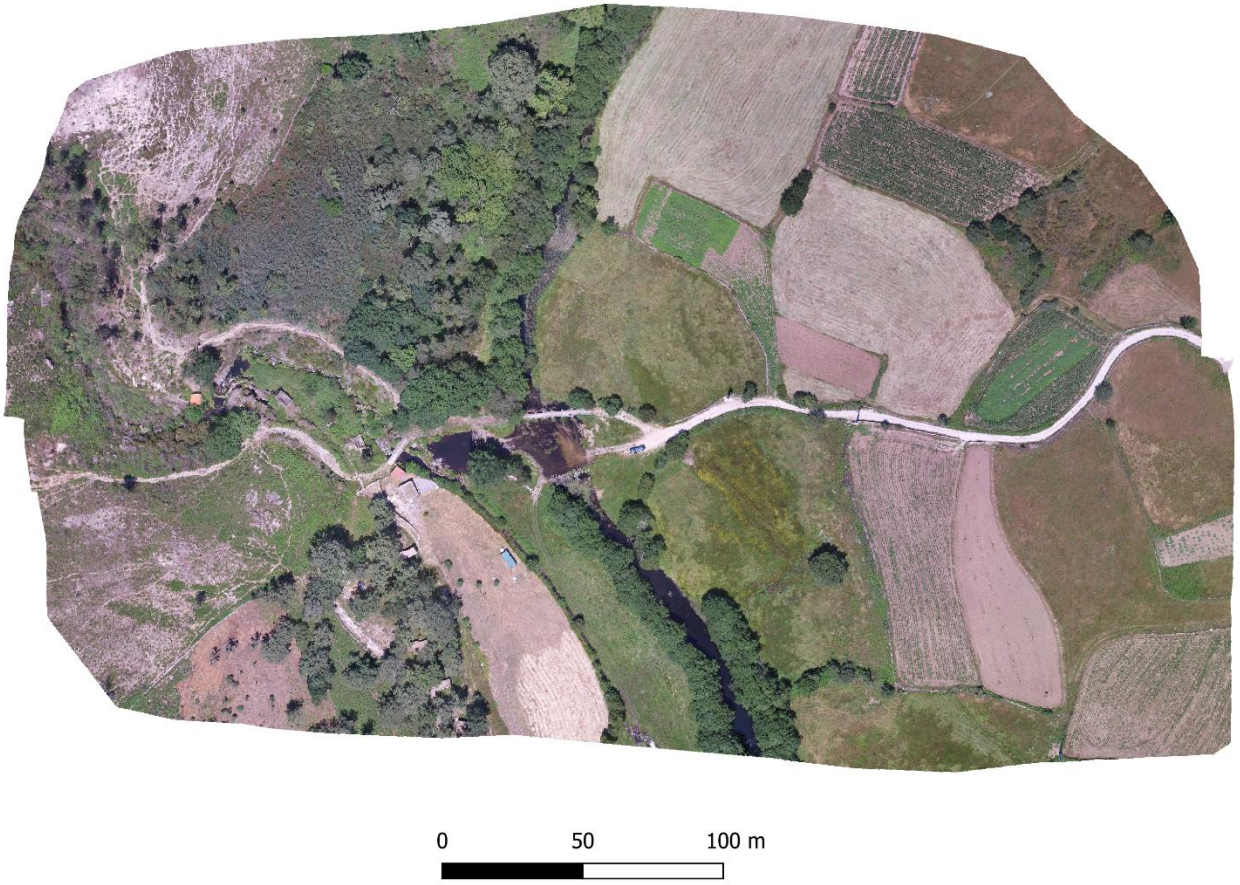

Figure I B. RAB2 stream reach orthophoto.

Figure I C. VEZ2 stream reach orthophoto.

Figure I D. VEZ3 stream reach orthophoto.

ANNEX II - NDVI maps of study sites based on UAV images

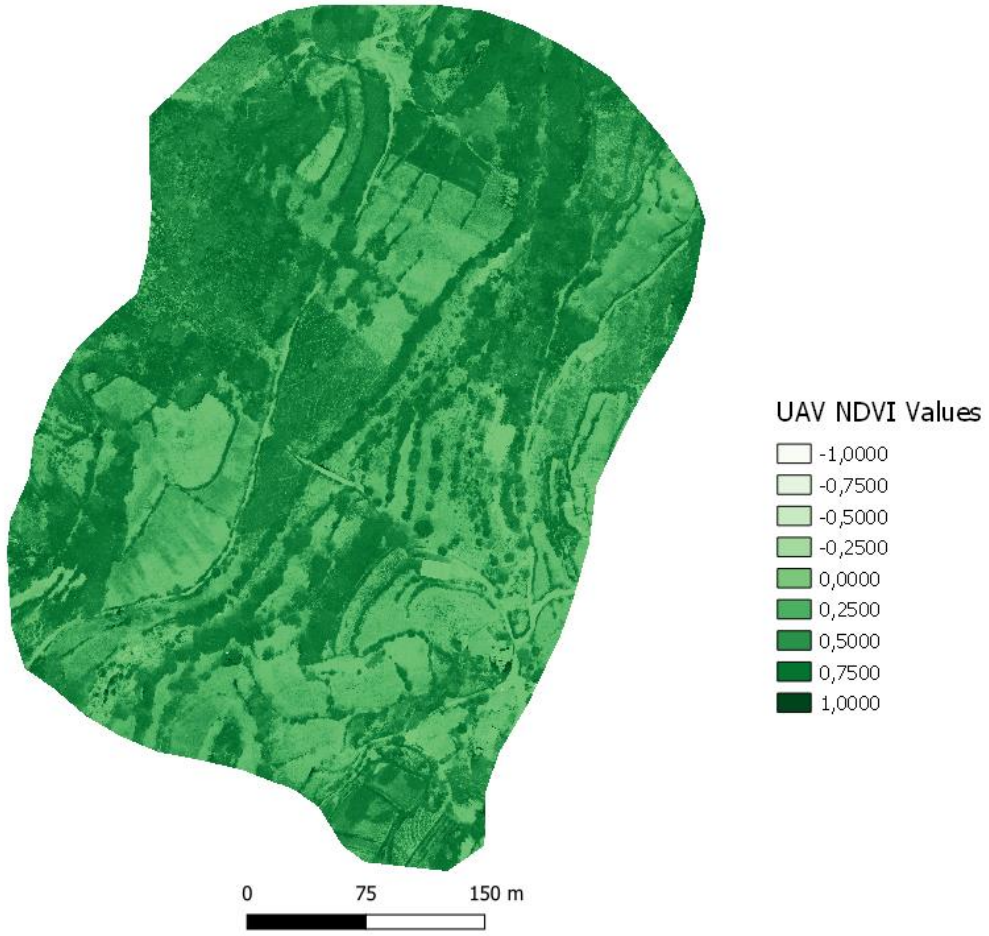

Figure II A. CAB1 stream reach UAV NDVI map.

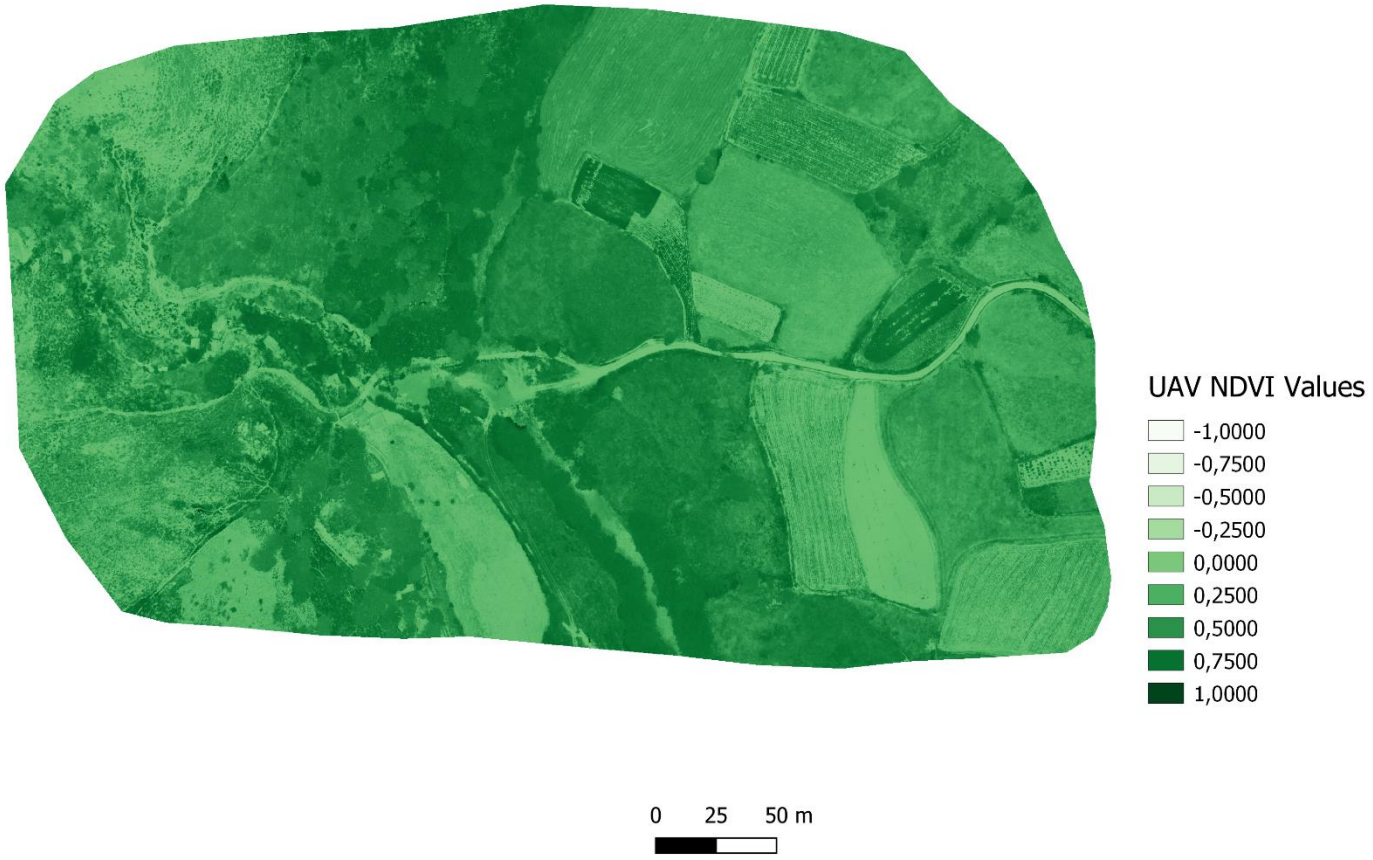

Figure II B. RAB2 stream reach UAV NDVI map.

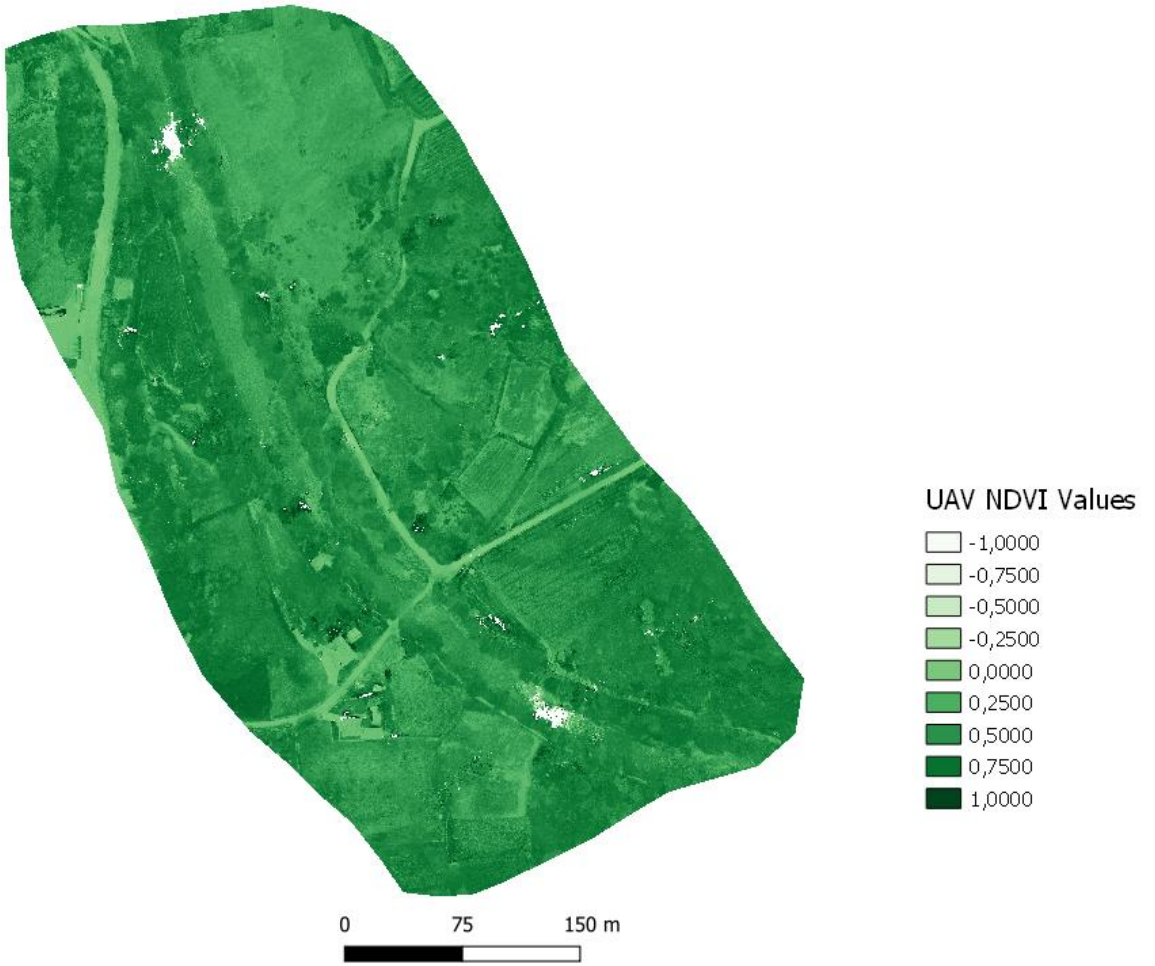

Figure II C. VEZ2 stream reach UAV NDVI map.

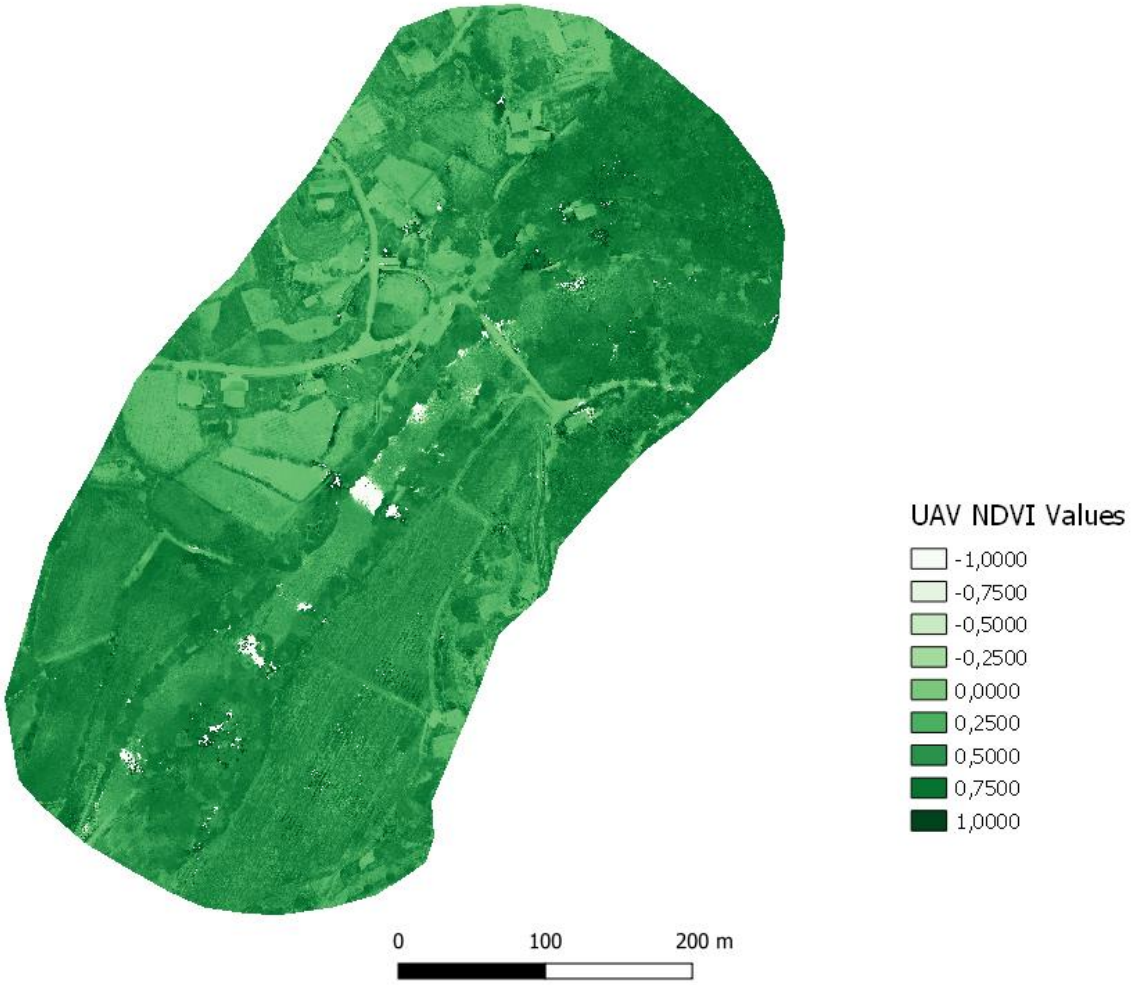

Figure II D. VEZ3 stream reach UAV NDVI map.

ANNEX III – NDVI maps of study sites based on Sentinel-2 images

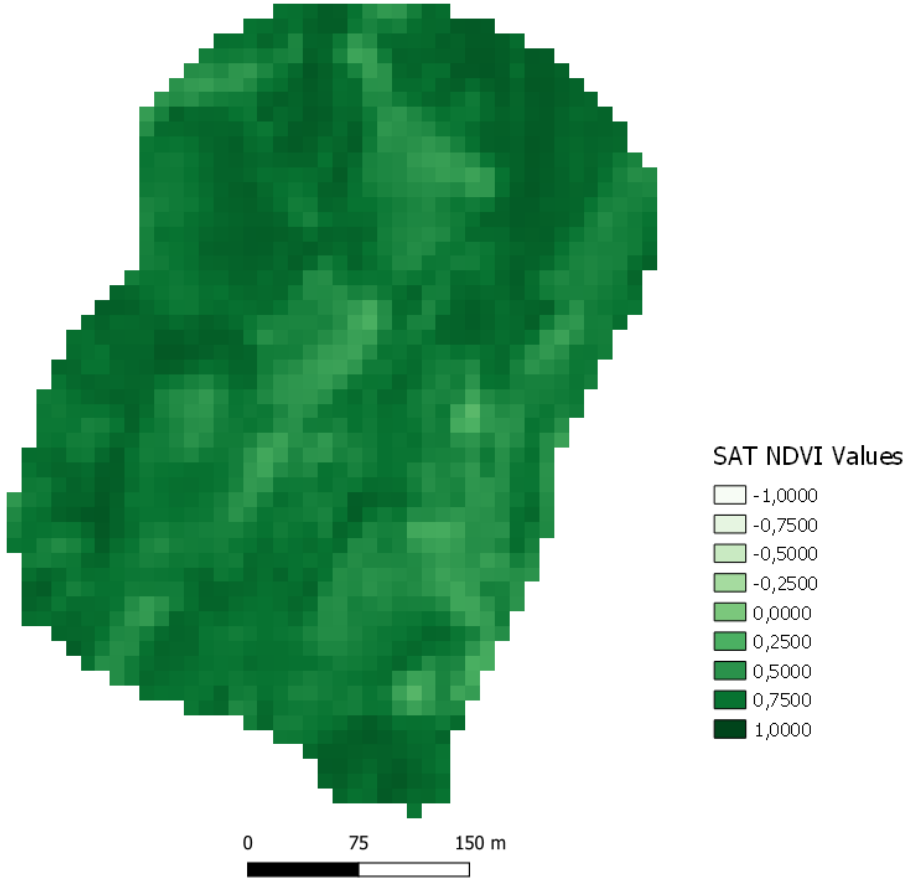

Figure III A. CAB1 stream reach Sentinel-2 NDVI map.

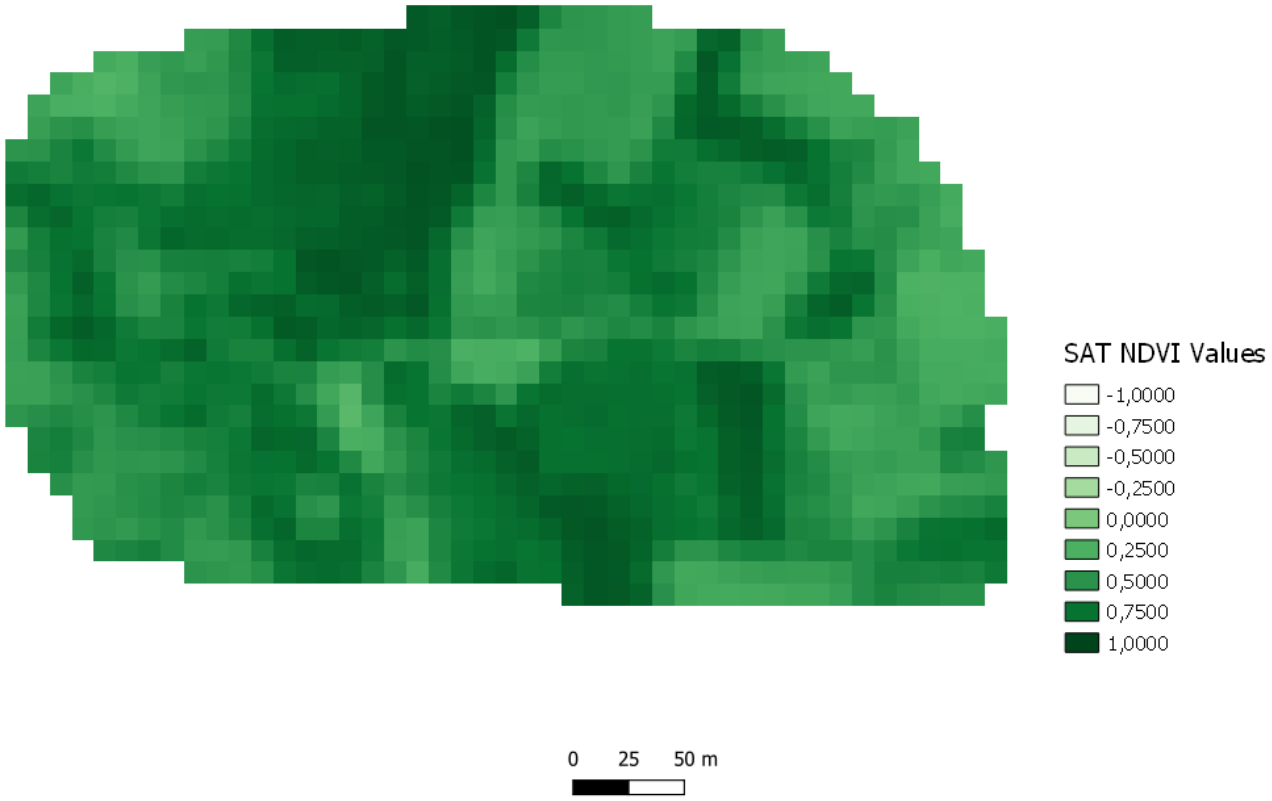

Figure III B. RAB2 stream reach Sentinel-2 NDVI map.

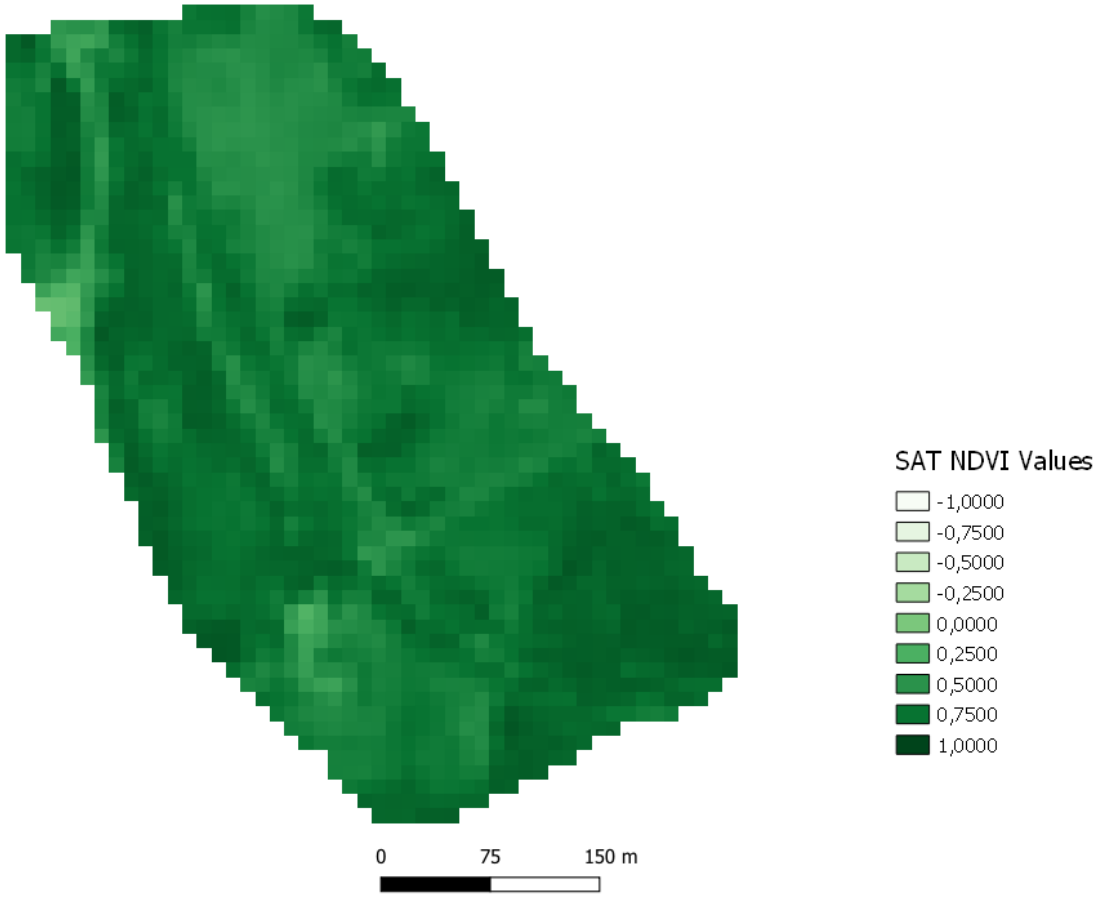

Figure III C. VEZ2 stream reach Sentinel-2 NDVI map.

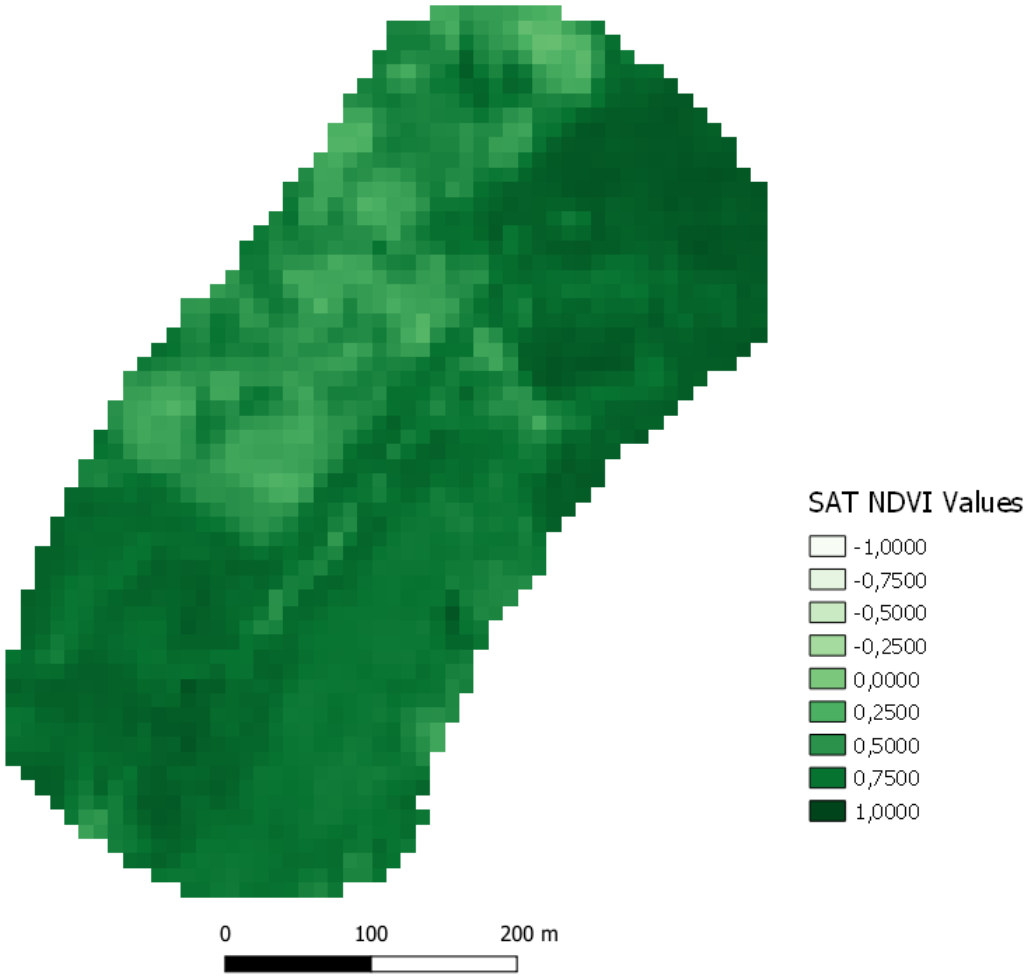

Figure III D. VEZ3 stream reach Sentinel-2 NDVI map.

ANNEX IV – Land cover maps of study sites

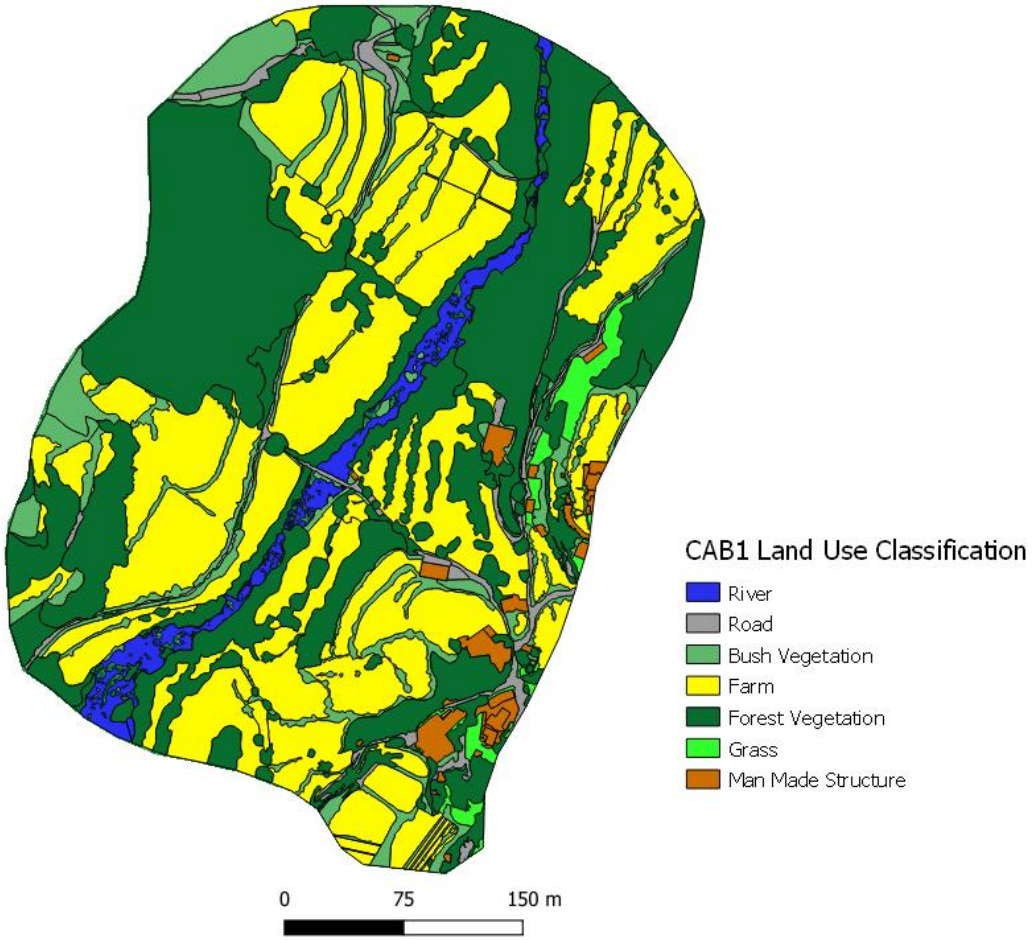

Figure IV A. Land cover classification map of CAB1.

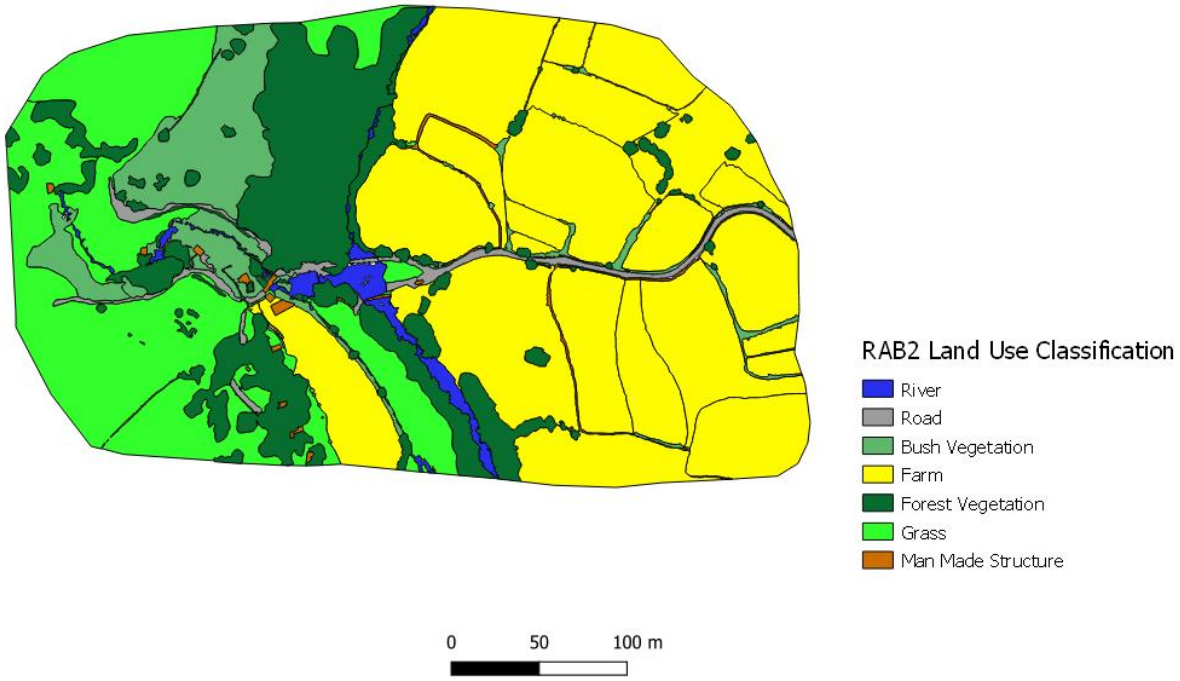

Figure IV B. Land cover classification map of RAB2.

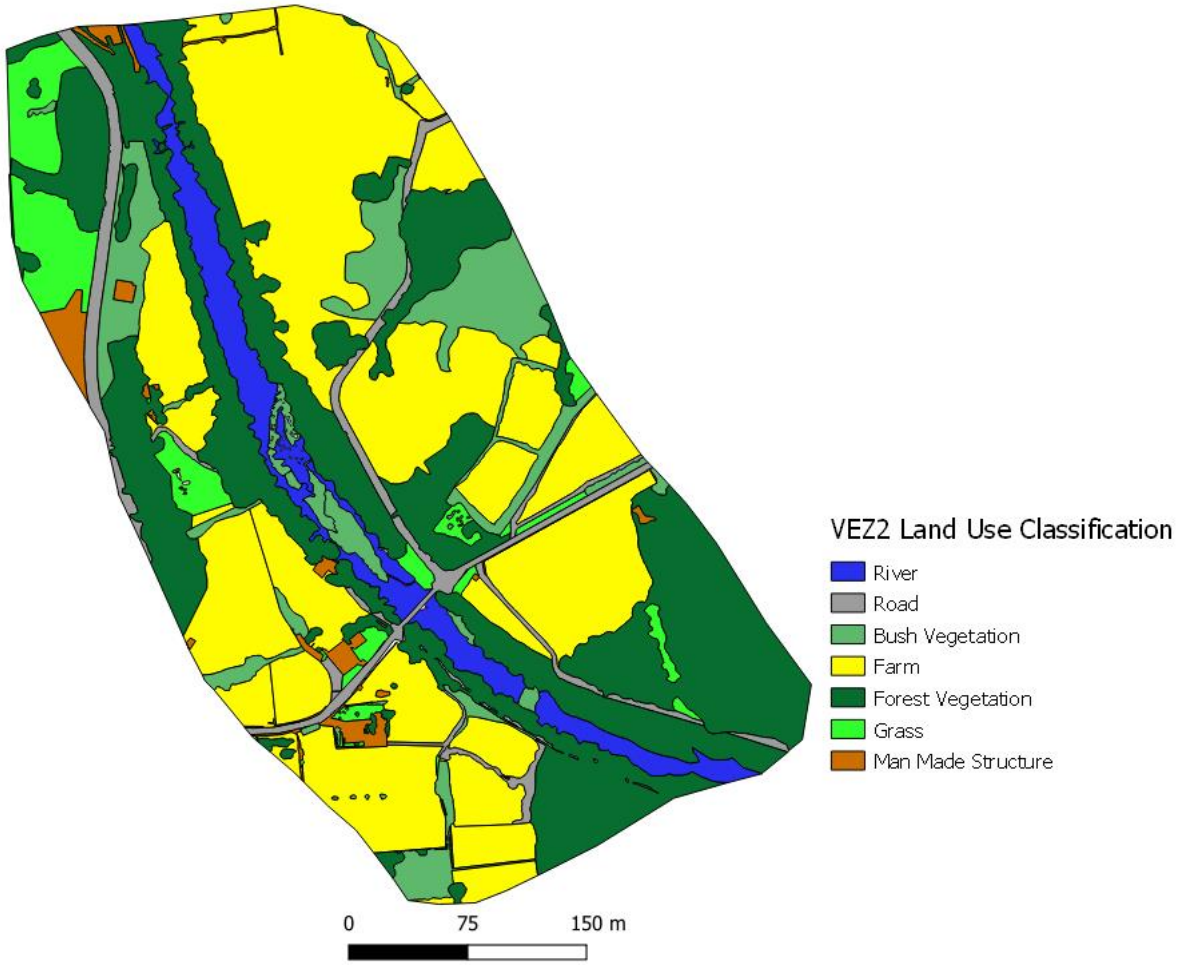

Figure IV C. Land cover classification map of VEZ2.

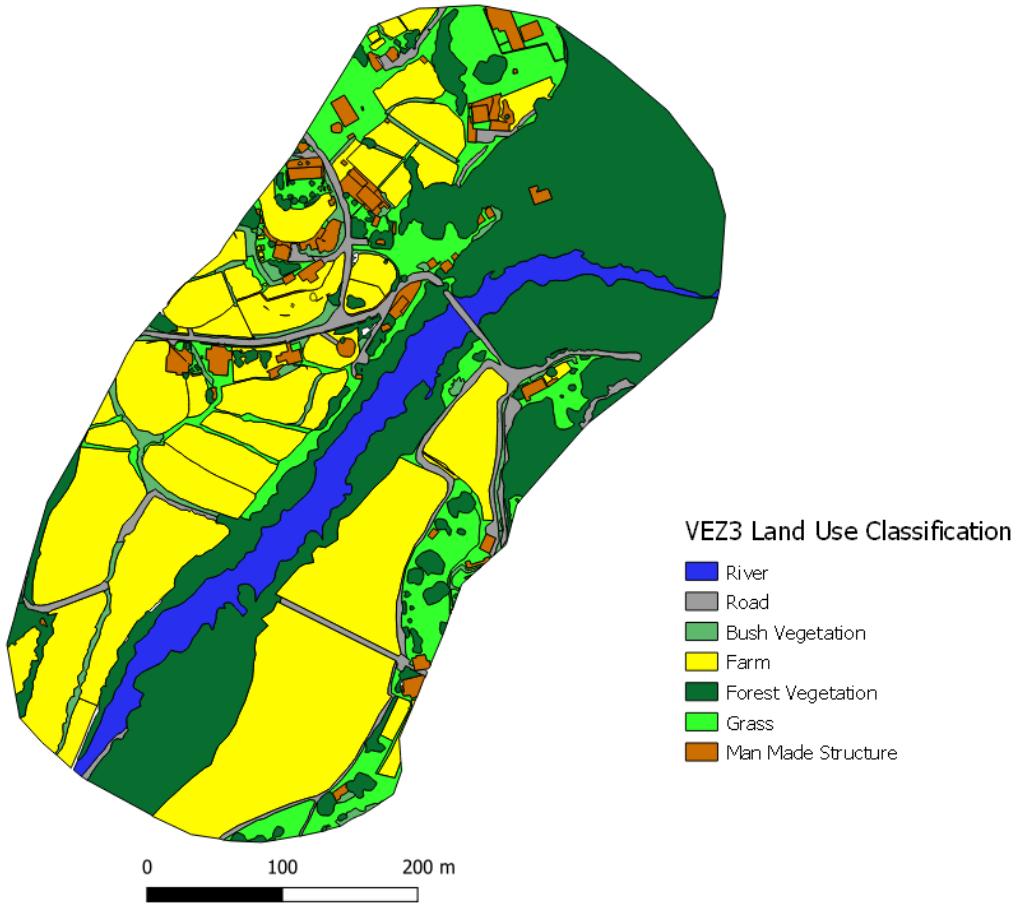

Figure IV D. Land cover classification map of VEZ3.

ANNEX V – Histograms of NDVI values

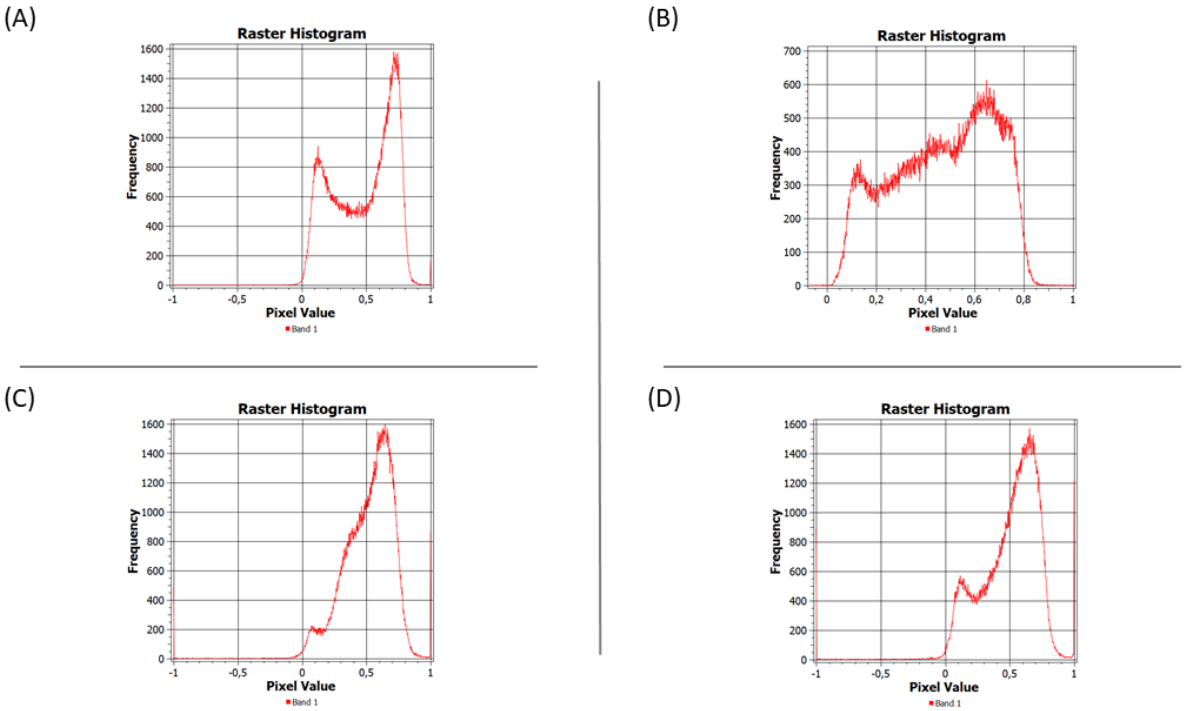

Figure V A. Histograms of UAV native resolution NDVI values. (A), (B), (C) and (D) correspond to CAB1, RAB2, VEZ2 and VEZ3, respectively.

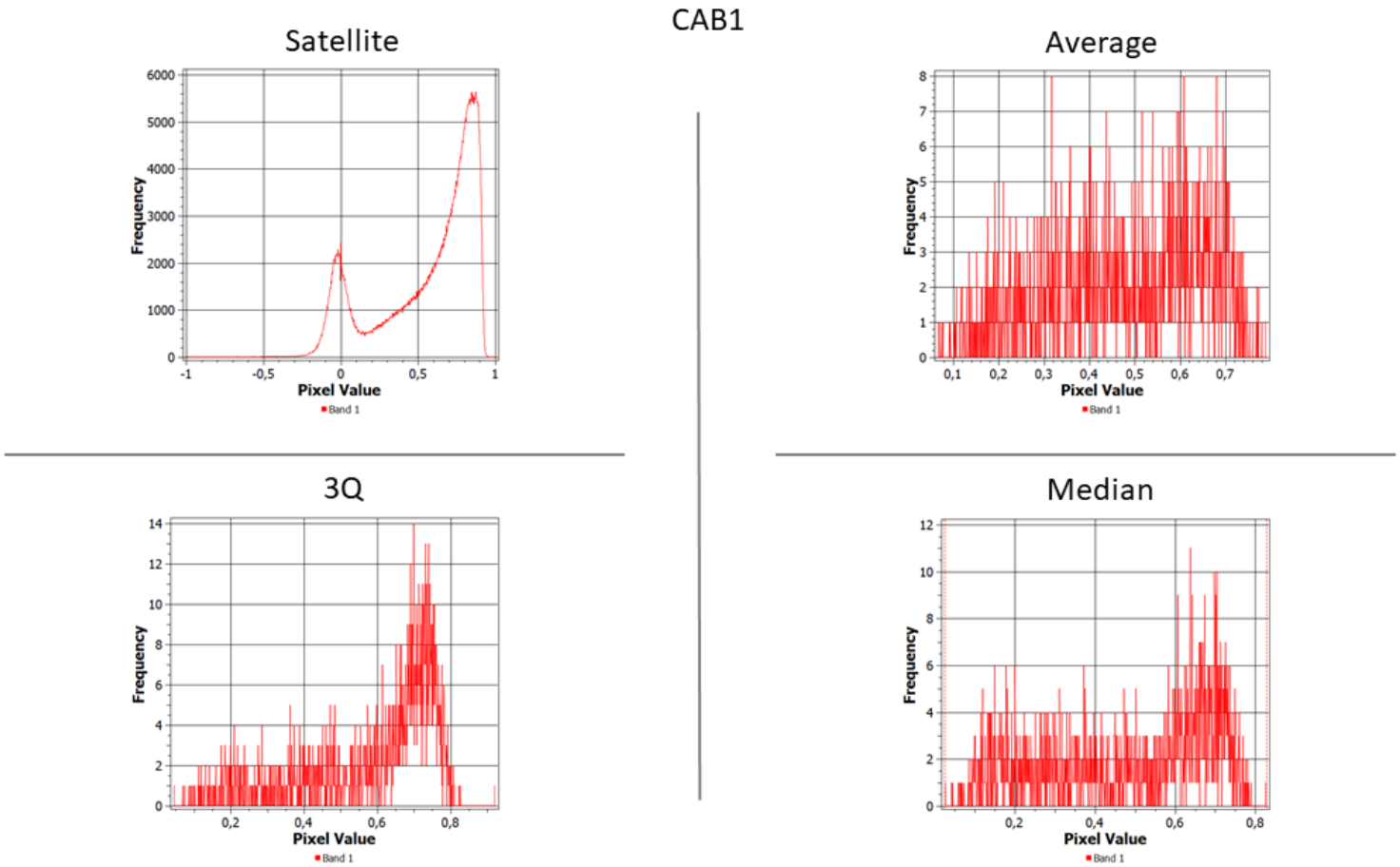

Figure V B. Histograms of NDVI values found in satellite and UAV rescaled images at CAB1.

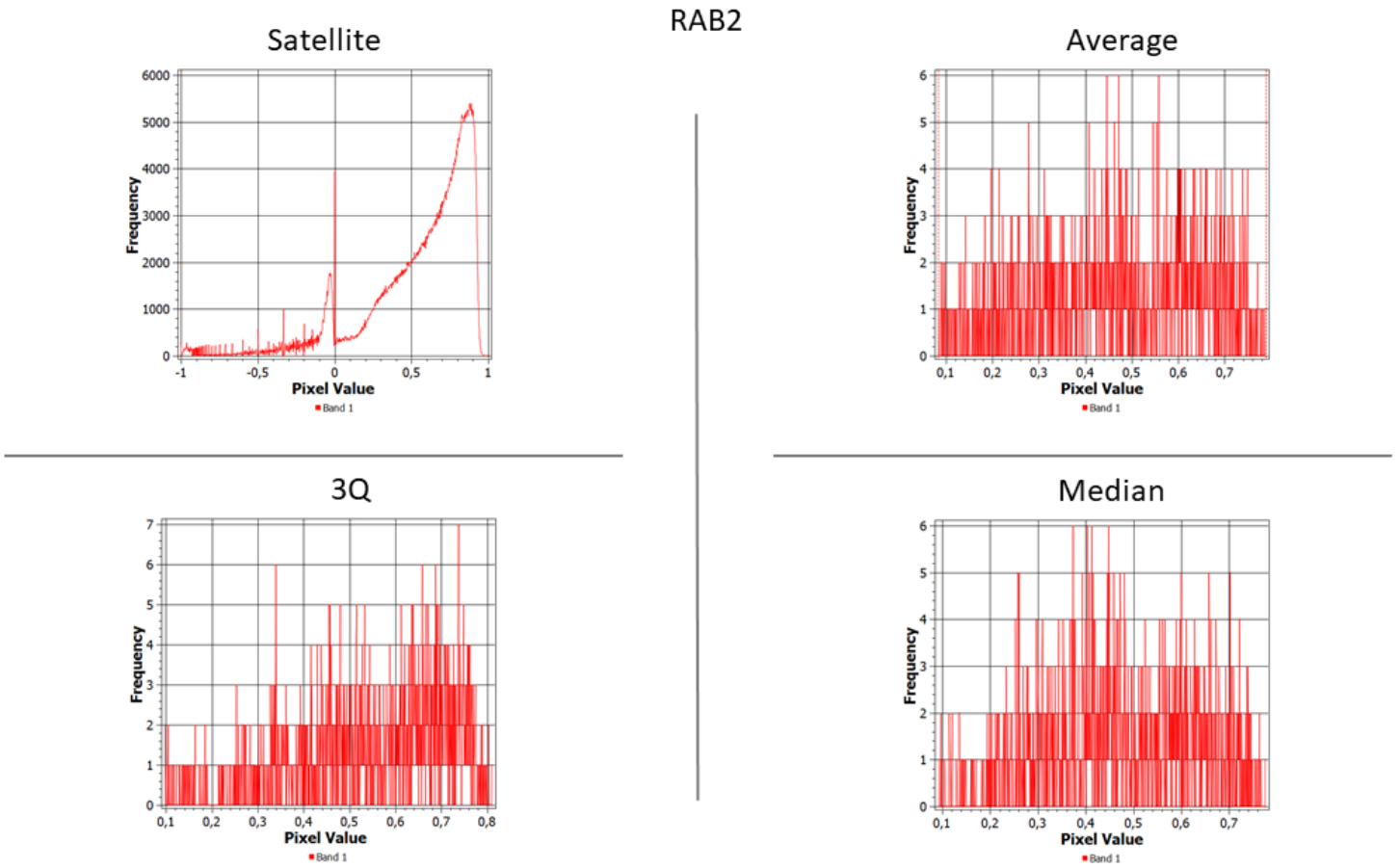

Figure V C. Histograms of NDVI values found in satellite and UAV rescaled images at RAB2.

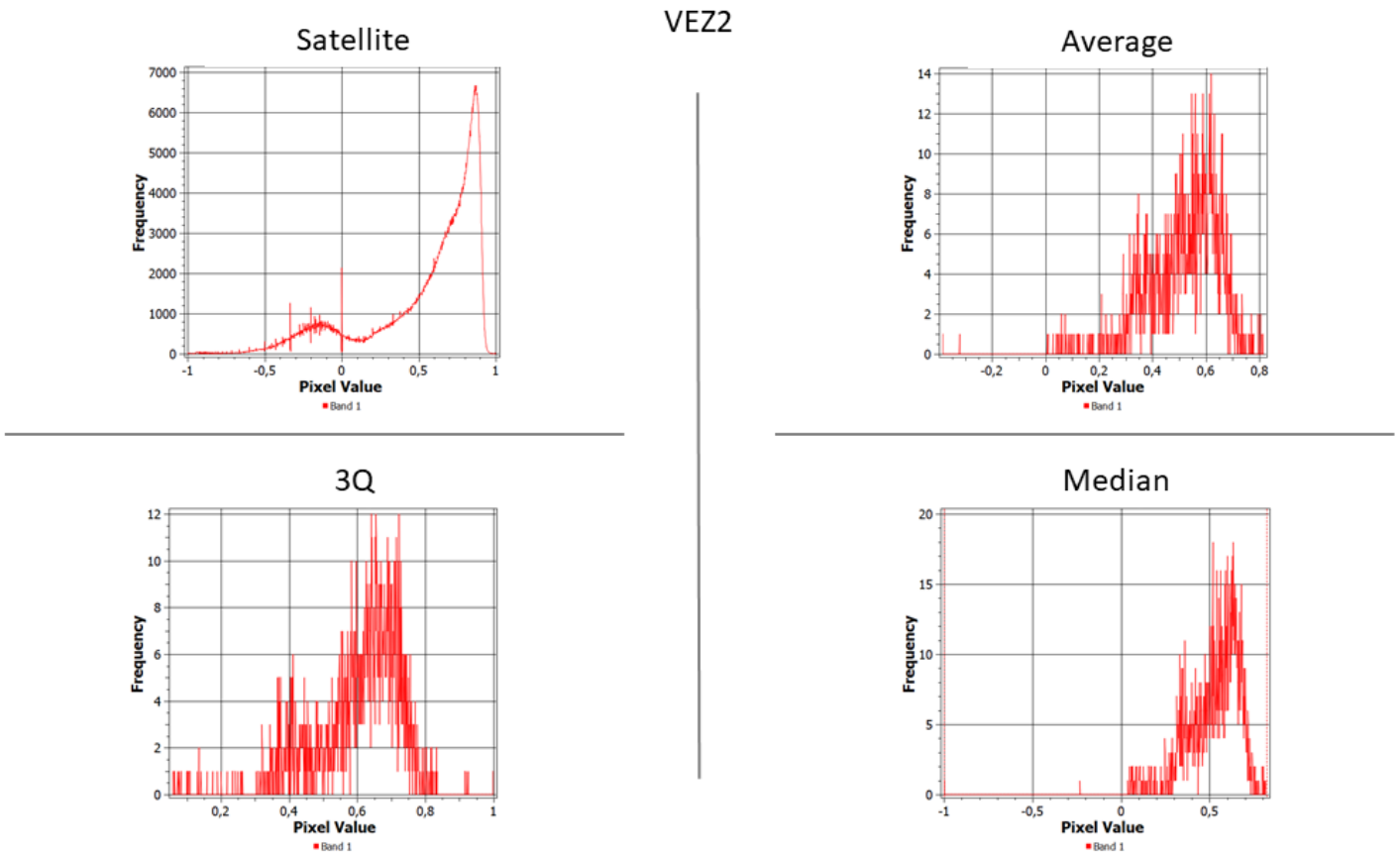

Figure V D. Histograms of NDVI values found in satellite and UAV rescaled images at VEZ2.

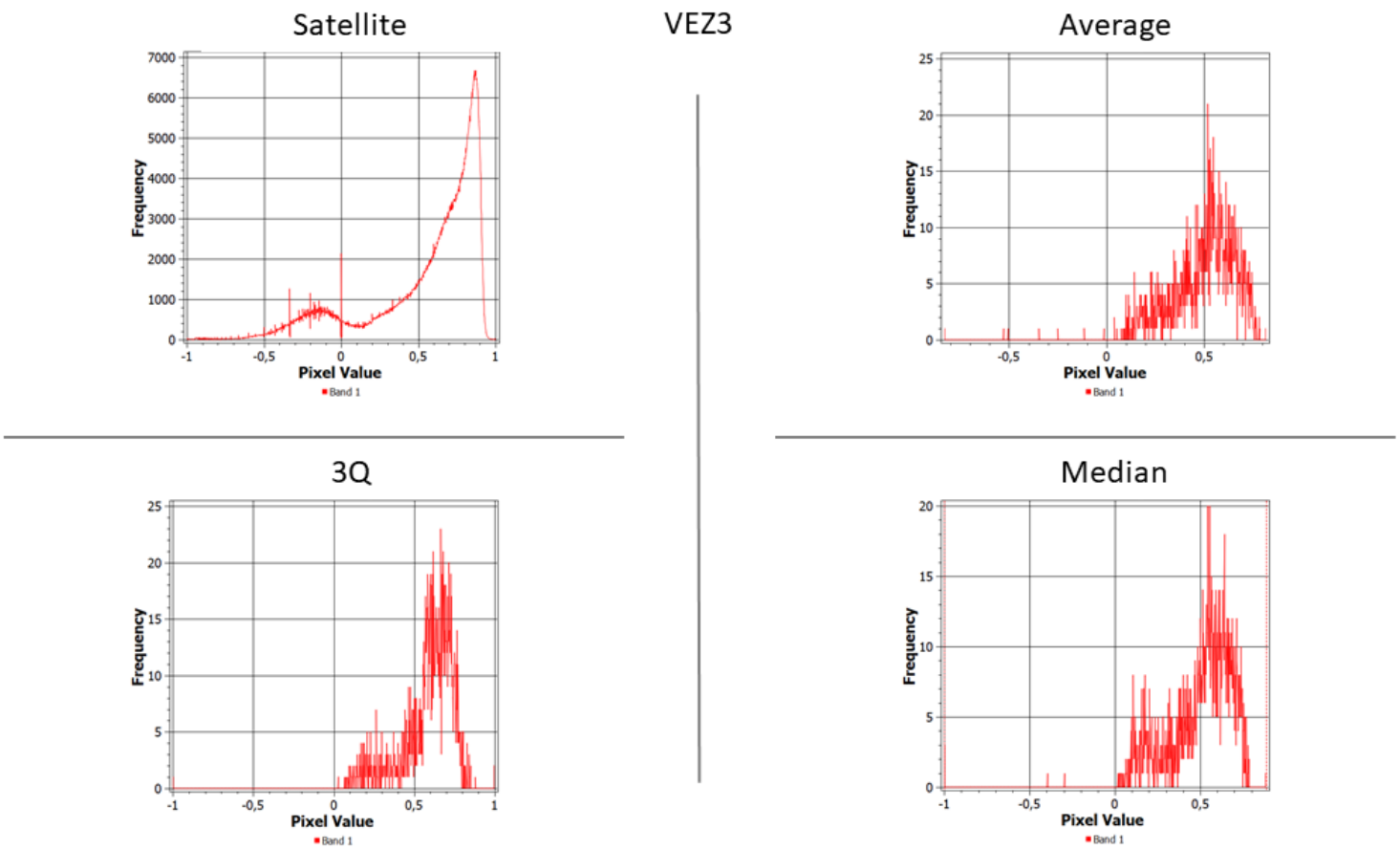

Figure V E. Histograms of NDVI values found in satellite and UAV rescaled images at VEZ3.

ANNEX VI - Results on linear regression models with land cover and river as predictor variables

Table VI A. Results of linear regression model applied to native.

	Estimate	Std. Error	t value
Intercept	0.241	0.008	31.764
ndvi_sat	0.442	0.009	51.044
RAB2	0.047	0.004	13.359
VEZ2	0.046	0.003	13.548
VEZ3	0.046	0.004	12.797
Farm	-0.122	0.005	-25.261
Forest	0.016	0.005	3.115
Grass	-0.125	0.006	-20.733
Manmade	-0.3	0.01	-31.06
River	-0.243	0.007	-33.404
Road	-0.316	0.008	-37.182
R2	0.387		
p value	< 2.2e-16		

Table VI B. Results of linear regression model applied to 3Q algorithm.

	Estimate	Std. Error	t value
Intercept	0.276	0.005	51.598
ndvi_sat	0.511	0.006	83.766
RAB2	-0.002	0.003	-0.908
VEZ2	-0.006	0.002	-2.369
VEZ3	-0.004	0.003	-1.66
Farm	-0.064	0.003	-18.805
Forest	0.016	0.004	4.578
Grass	-0.037	0.004	-8.733
Manmade	-0.115	0.007	-16.932
River	-0.092	0.005	-17.995
Road	-0.034	0.006	-5.703
R2	0.437		
p value	< 2.2e-16		

Table VI C. Results of linear regression model applied to MN algorithm.

	Estimate	Std. Error	t value
Intercept	0.114	0.007	16.722
ndvi_sat	0.561	0.008	71.891
RAB2	0.047	0.003	14.703
VEZ2	0.036	0.003	11.697
VEZ3	0.029	0.003	8.997
Farm	-0.046	0.004	-10.673
Forest	0.028	0.005	6.299
Grass	-0.062	0.005	-11.459
Manmade	-0.134	0.009	-15.404
River	-0.108	0.007	-16.562
Road	-0.076	0.008	-9.933
R2	0.367		
p value	< 2.2e-16		

Table VI D. Results of linear regression model applied to AV algorithm.

	Estimate	Std. Error	t value
Intercept	0.122	0.005	24.271
ndvi_sat	0.528	0.006	92.155
RAB2	0.038	0.002	16.117
VEZ2	0.027	0.002	11.919
VEZ3	0.0215	0.002	8.975
Farm	-0.028	0.003	-8.645
Forest	0.041	0.003	12.452
Grass	-0.042	0.004	-10.511
Manmade	-0.1	0.006	-15.608
River	-0.098	0.005	-20.322
Road	-0.065	0.006	-6.016
R2	0.483		
p value	< 2.2e-16		

ANNEX VII – Point dispersion plots for UAV rescaled images

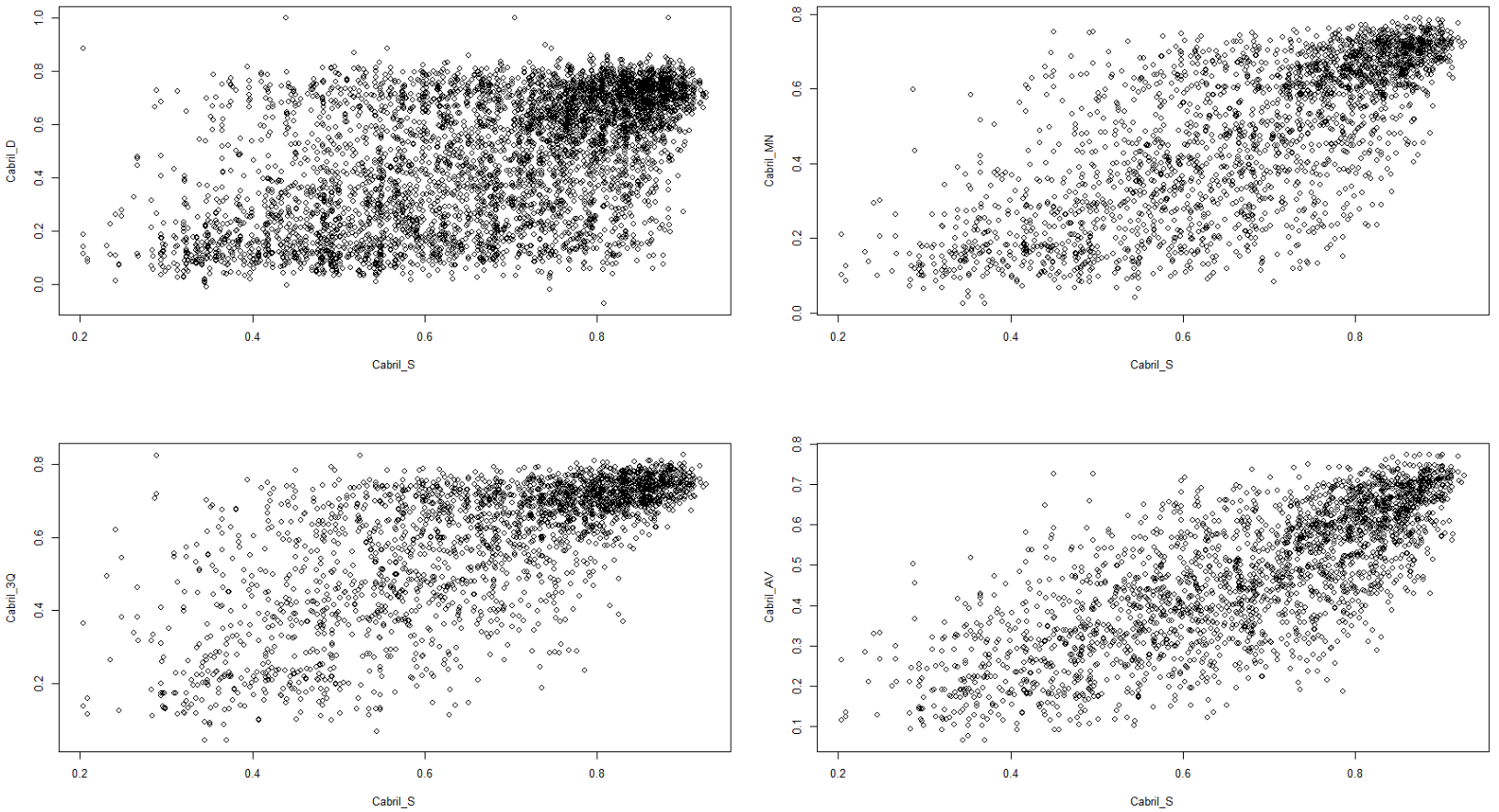

Figure VII A. Comparison between UAV and satellite NDVI values at native and rescaled resolutions in CAB1.

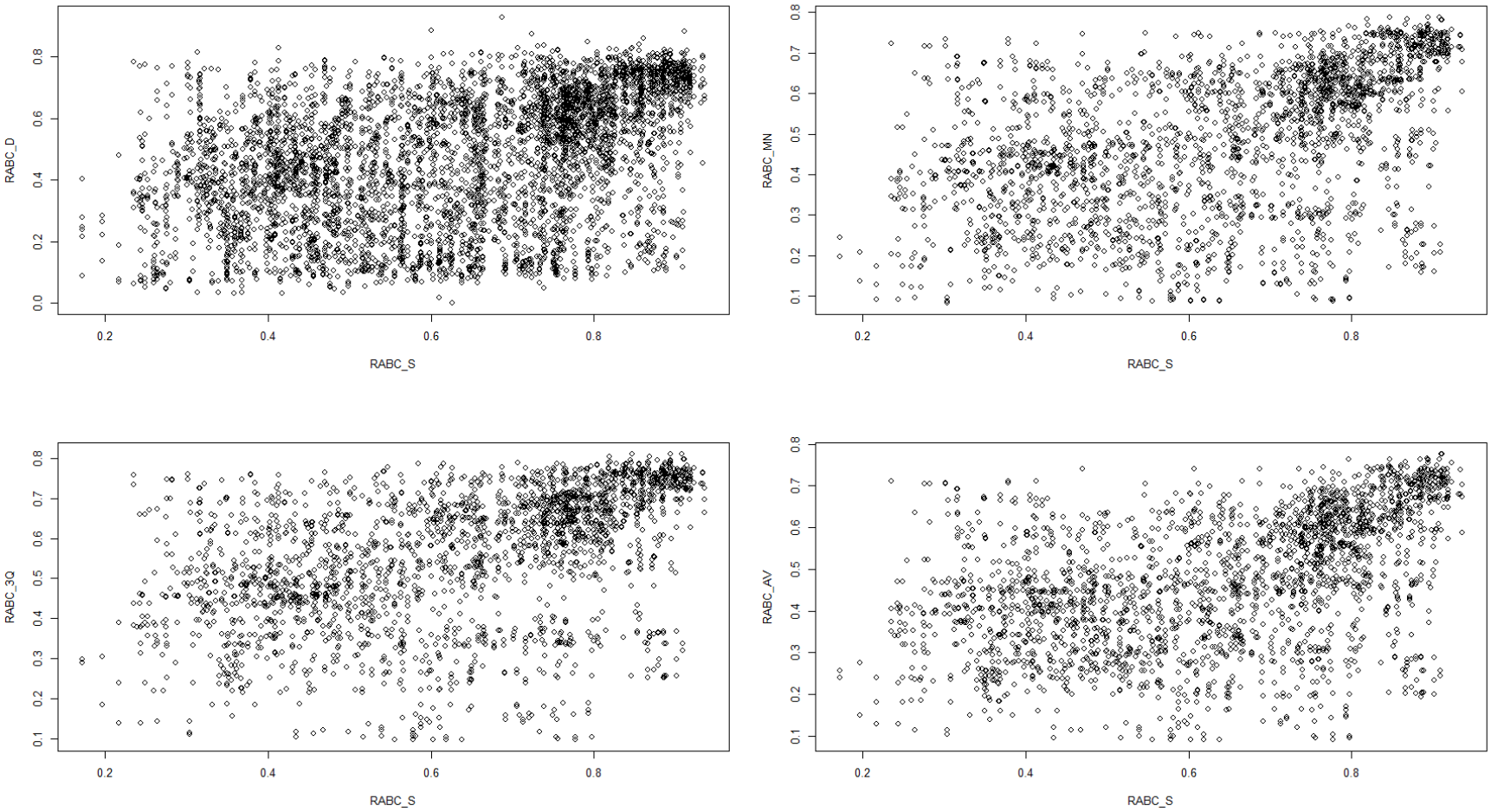

Figure VII B. Comparison between UAV and satellite NDVI values at native and rescaled resolutions in RAB2.

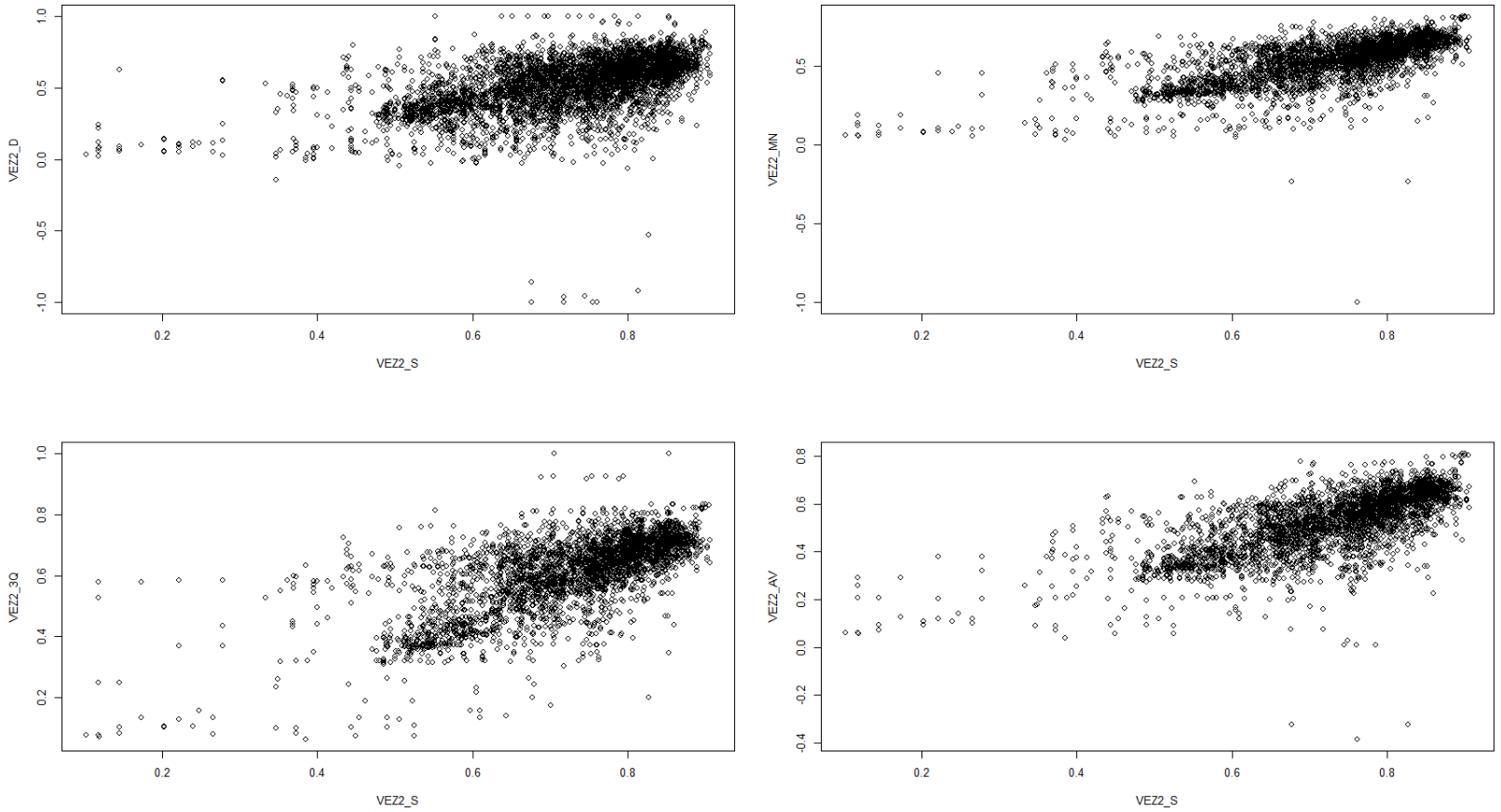

Figure VII C. Comparison between UAV and satellite NDVI values at native and rescaled resolutions in VEZ2.

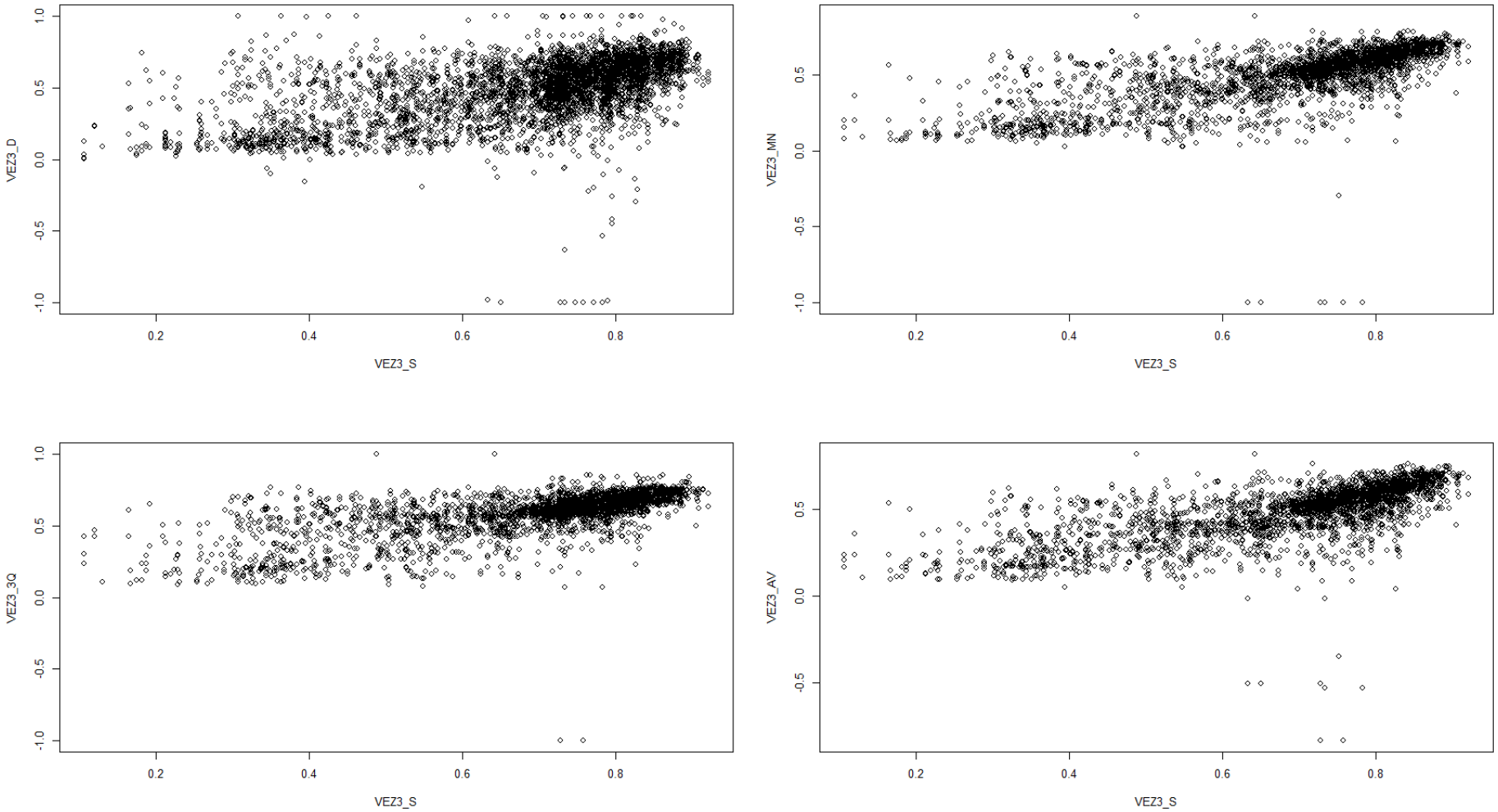

Figure VII D. Comparison between UAV and satellite NDVI values at native and rescaled resolutions in RAB2.

ANNEX VIII - Stacked column chart for land cover based on R^2 measurements

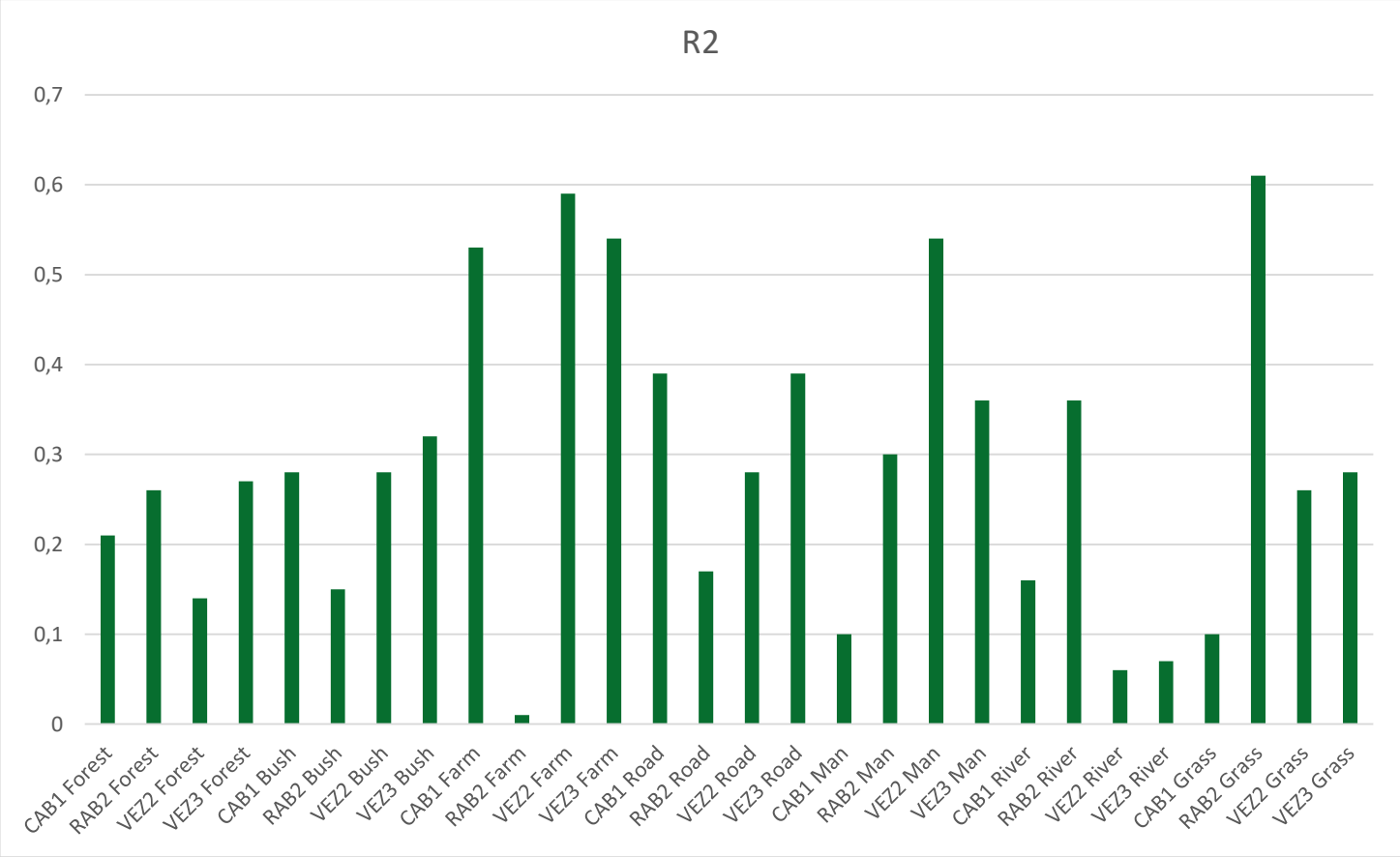

Figure VIII A. Stacked column chart for land cover based on R2 measurements.

ANNEX IX – Land cover occupancy by polygon n.º and area

Table IX A. Land cover occupancy values in % and n.° of polygons at all river reaches.

Polygons		CAB1	RAB2	VEZ2	VEZ3
	Forest	167	140	32	90
	Bush	118	94	41	44
	Farm	98	43	28	54
	Grass	19	39	24	50
	Road	81	40	35	16
	River	26	61	42	2
	Man Made	48	108	74	89
	Total	557	525	276	345

Polygons (%)		CAB1	RAB2	VEZ2	VEZ3
	Forest	29.98%	26.67%	11.59%	26.08%
	Bush	21.18%	17.90%	14.86%	12.75%
	Farm	17.59%	8.19%	10.15%	15.65%
	Grass	3.41%	7.43%	8.70%	14.49%
	Road	14.54%	7.62%	12.68%	4.64%
	River	4.67%	11.62%	15.22%	0.58%
	Man Made	8.62%	20.57%	26.81%	25.80%
	Total	100%	100%	100%	100%

Area (m2)		CAB1	RAB2	VEZ2	VEZ3
	Forest	67842.07	18405.76	55173.65	64580.54
	Bush	16246.92	8872.642	13882.71	4752.876
	Farm	62162.73	51816.81	67590.93	70919.79
	Grass	2352.946	22665.53	8885.807	21055.28
	Road	5058.588	1969.321	7749.512	8261.887
	River	4732.552	1940.257	9445.27	12616.07
	Man Made	3270.591	1047.685	3178.531	6728.085
	Total	161666.4	106718	165906.4	188914.5

Area (%)		CAB1	RAB2	VEZ2	VEZ3
	Forest	41.96%	17.25%	33.26%	34.19%
	Bush	10.05%	8.31%	8.37%	2.52%
	Farm	38.45%	48.55%	40.74%	37.54%
	Grass	1.46%	21.24%	5.36%	11.15%
	Road	3.13%	1.85%	4.67%	4.37%
	River	2.93%	1.82%	5.69%	6.68%
	Man Made	2.02%	0.98%	1.92%	3.56%
	Total	100%	100%	100%	100%

ANNEX X – Facet wraps plots of value dispersion taking land cover into account.

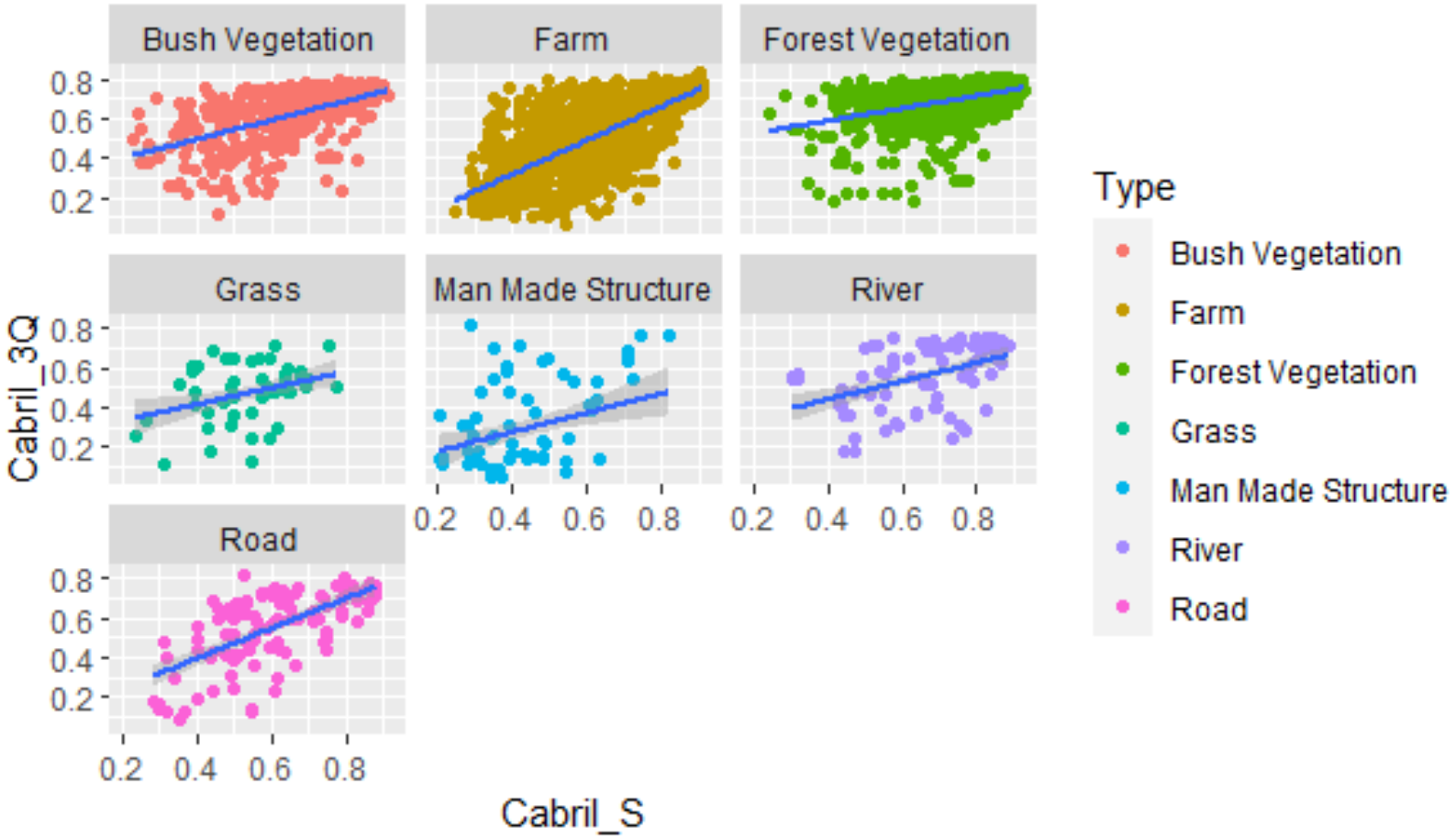

Figure X A. Facet graph plot for CAB1.

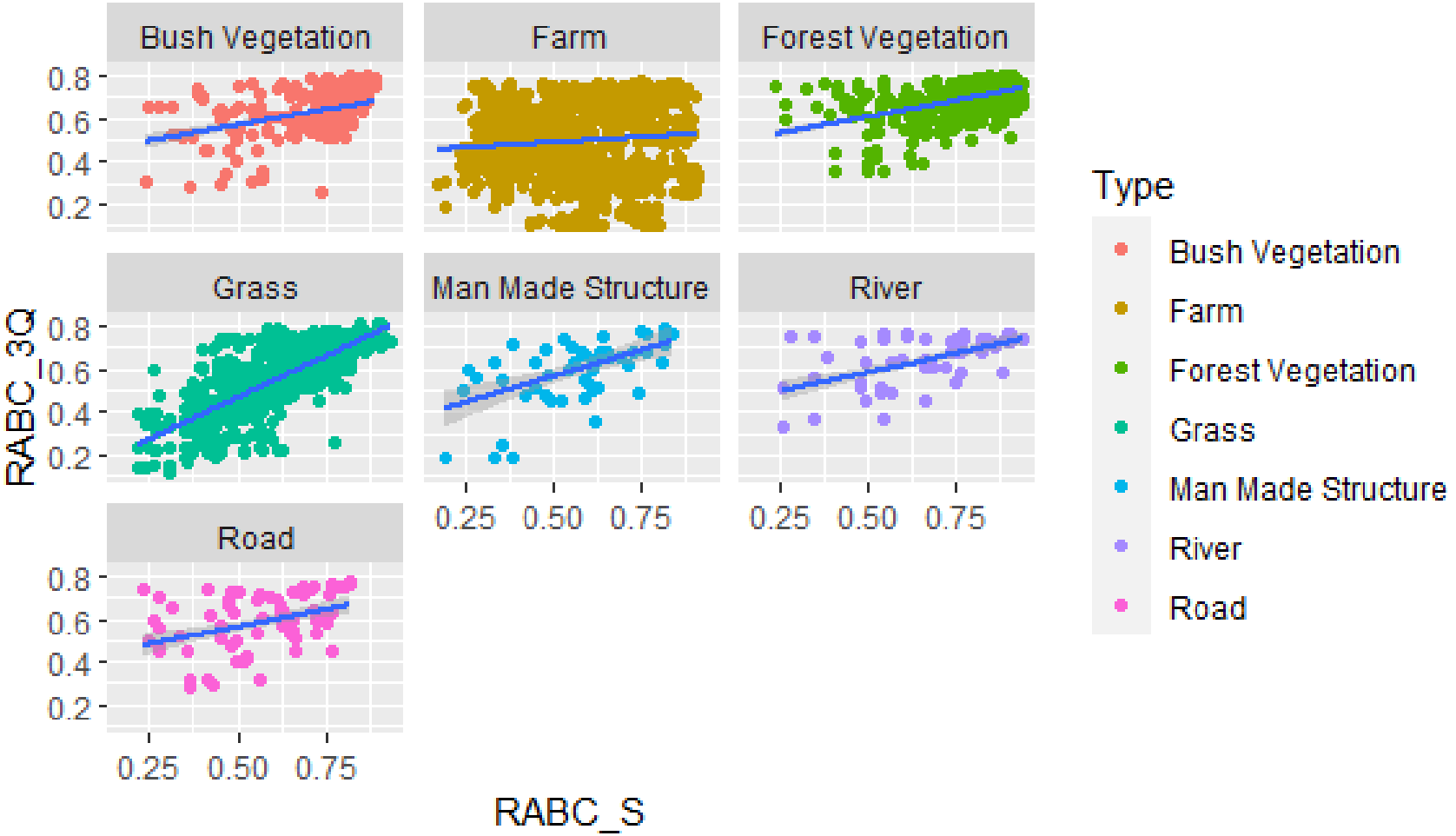

Figure X B. Facet graph plot for CAB1.

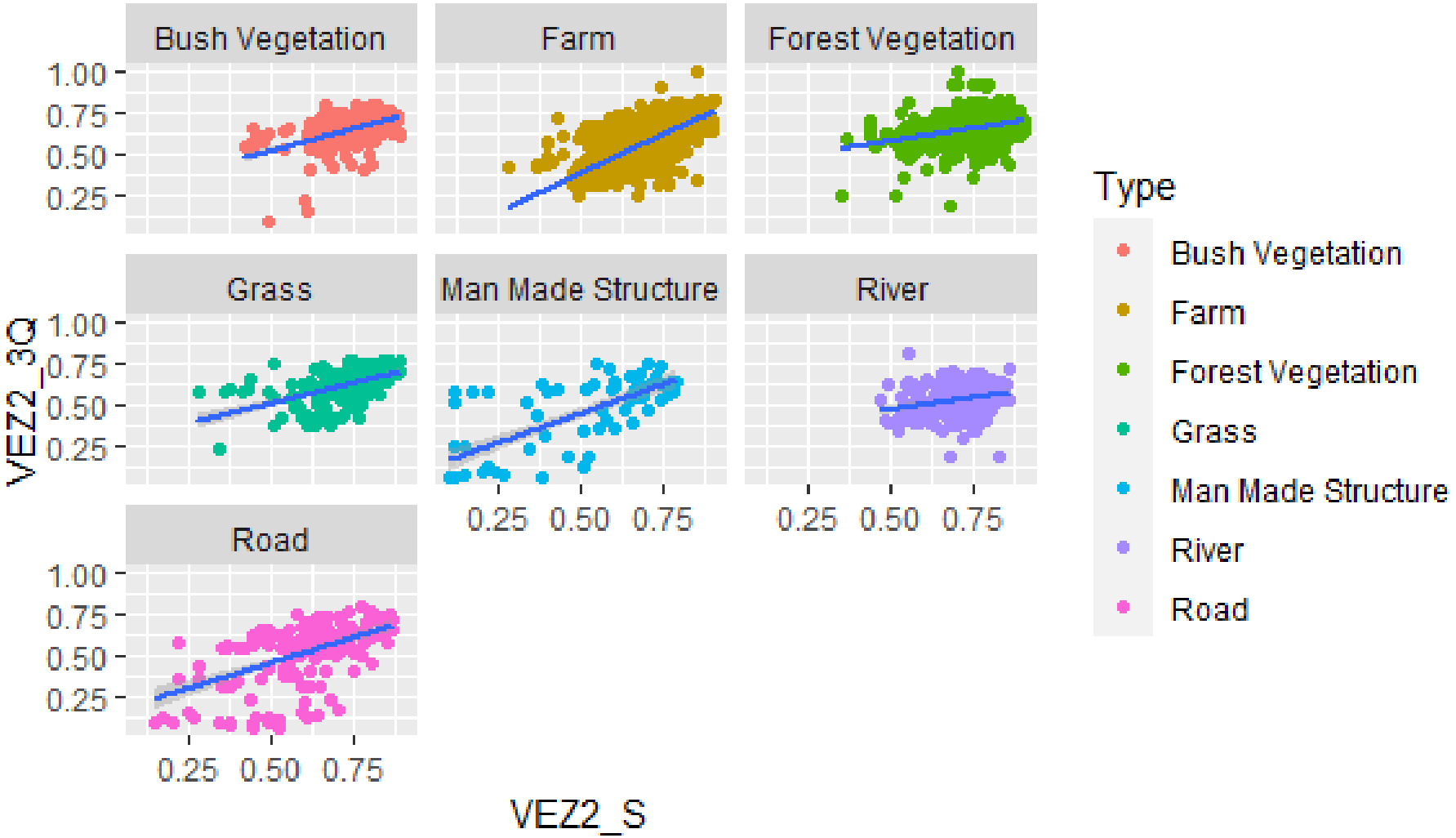

Figure X C. Facet graph plot for VEZ2.

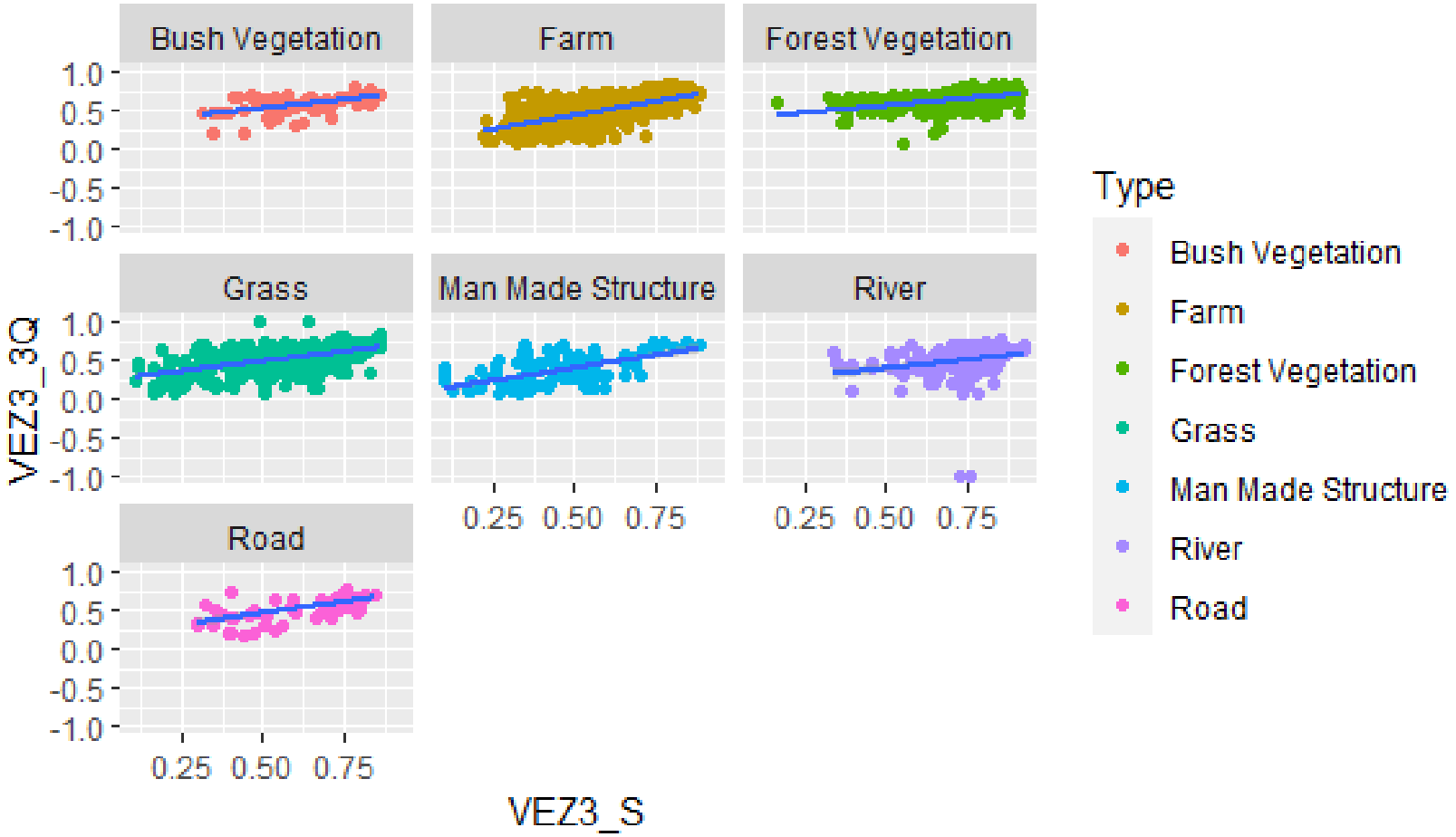

Figure X D. Facet graph plot for VEZ3.

BIBLIOGRAPHY

Abdullah, M. M., Al-Ali, Z. M., & Srinivasan, S. (2021). The use of UAV-based remote sensing to estimate biomass and carbon stock for native desert shrubs. *MethodsX*, *8*, 101399. https://doi.org/10.1016/j.mex.2021.101399

Afroz, R., & Rahman, A. (2017). Health impact of river water pollution in Malaysia. *International Journal of ADVANCED AND APPLIED SCIENCES*, *4*, 78–85. https://doi.org/10.21833/ijaas.2017.05.014

Agência Portuguesa do Ambiente. (2019). *Classificação das massas de água: Avaliação intercalar 2017-2019*. https://www.apambiente.pt/agua/estado-das-massas-de-agua

Alleaume, S., Dusseux, P., Thierion, V., Commagnac, L., Laventure, S., Lang, M., Féret, J.-B., Hubert-Moy, L., & Luque, S. (2018). A generic remote sensing approach to derive operational essential biodiversity variables (EBVs) for conservation planning. *Methods in Ecology and Evolution*, *9*(8), 1822–1836. https://doi.org/10.1111/2041-210X.13033

Alvarez-Vanhard, E., Houet, T., Mony, C., Lecoq, L., & Corpetti, T. (2020). Can UAVs fill the gap between in situ surveys and satellites for habitat mapping? *Remote Sensing of Environment*, *243*, 111780. https://doi.org/10.1016/j.rse.2020.111780

Asner, G. P. (1998). Biophysical and Biochemical Sources of Variability in Canopy Reflectance. *Remote Sensing of Environment*, *64*(3), 234–253. https://doi.org/10.1016/S0034-4257(98)00014-5

Atzberger, C. (2013). Advances in Remote Sensing of Agriculture: Context Description, Existing Operational Monitoring Systems and Major Information Needs. *Remote Sensing*, *5*(2), 949–981. https://doi.org/10.3390/rs5020949

Bansod, B., Singh, R., Thakur, R., & Singhal, G. (2017). A comparision between satellite based and drone based remote sensing technology to achieve sustainable development: A review. *Journal of Agriculture and Environment for International Development (JAEID)*, *111*(2). https://doi.org/10.12895/jaeid.20172.690

Barton, C. V. M. (2012). Advances in remote sensing of plant stress. *Plant and Soil*, *354*(1–2), 41–44. https://doi.org/10.1007/s11104-011-1051-0

Beisel, N. S., Callaham, J. B., Sng, N. J., Taylor, D. J., Paul, A.-L., & Ferl, R. J. (2018). Utilization of single-image normalized difference vegetation index (SI-NDVI) for early plant stress detection. *Applications in Plant Sciences*, *6*(10), e01186. https://doi.org/10.1002/aps3.1186

Berni, J., Zarco-Tejada, P. J., Suarez, L., & Fereres, E. (2009). Thermal and Narrowband Multispectral Remote Sensing for Vegetation Monitoring From an Unmanned Aerial Vehicle. *IEEE Transactions on Geoscience and Remote Sensing*, *47*(3), 722–738. https://doi.org/10.1109/TGRS.2008.2010457

Bertini, F., Brand, O., Carlier, S., Del Bello, U., Drusch, M., Duca, R., Fernandez, V., Ferrario, C., Ferreira, M. H., Isola, C., Kirschner, V., Laberinti, P., Lambert, M., Mandorlo, G., Marcos, P., Martimort, P., Moon, S., Oldeman, P., Palomba, M., & Pineiro, J. (2012). Sentinel-2 ESA's Optical High-Resolution Mission for GMES Operational Services. *ESA Bulletin. Bulletin ASE. European Space Agency*, *SP-1322*.

Bodner, G. S., & Robles, M. D. (2017). Enduring a decade of drought: Patterns and drivers of vegetation change in a semi-arid grassland. *Journal of Arid Environments*, *136*, 1–14. https://doi.org/10.1016/j.jaridenv.2016.09.002

Bollas, N., Kokinou, E., & Polychronos, V. (2021). Comparison of Sentinel-2 and UAV Multispectral Data for Use in Precision Agriculture: An Application from Northern Greece. *Drones*, *5*(2), 35. https://doi.org/10.3390/drones5020035

Brekke, C., & Solberg, A. H. S. (2005). Oil spill detection by satellite remote sensing. *Remote Sensing of Environment*, *95*(1), 1–13. https://doi.org/10.1016/j.rse.2004.11.015

Breshears, D. D., Cobb, N. S., Rich, P. M., Price, K. P., Allen, C. D., Balice, R. G., Romme, W. H., Kastens, J. H., Floyd, M. L., Belnap, J., Anderson, J. J., Myers, O. B., & Meyer, C. W. (2005). Regional vegetation die-off in response to global-change-type drought. *Proceedings of the National Academy of Sciences*, *102*(42), 15144–15148. https://doi.org/10.1073/pnas.0505734102

Bruno, D., Gutiérrez-Cánovas, C., Sánchez-Fernández, D., Velasco, J., & Nilsson, C. (2016). Impacts of environmental filters on functional redundancy in riparian vegetation. *Journal of Applied Ecology*, *53*(3), 846–855. https://doi.org/10.1111/1365-2664.12619

Cai, N., Zhou, X., Yang, Y., Wang, J., Zhang, D., & Hu, R. (2018). Use of UAV images to assess narrow brown leaf spot severity in rice. *International Journal of Precision Agricultural Aviation*, *1*(1), 38–42. https://doi.org/10.33440/j.ijpaa.20190202.47

Casado, M., Gonzalez, R., Kriechbaumer, T., & Veal, A. (2015). Automated Identification of River Hydromorphological Features Using UAV High Resolution Aerial Imagery. *Sensors*, *15*(11), 27969–27989. https://doi.org/10.3390/s151127969

Cavur, M., Duzgun, H. S., Kemec, S., & Demirkan, D. C. (2019). LAND USE AND LAND COVER CLASSIFICATION OF SENTINEL 2-A: ST PETERSBURG CASE STUDY. *The International Archives of the Photogrammetry, Remote Sensing and Spatial Information Sciences*, *XLII-1/W2*, 13–16. https://doi.org/10.5194/isprs-archives-XLII-1-W2-13-2019

Ceccato, P., Flasse, S., Tarantola, S., Jacquemoud, S., & Grégoire, J.-M. (2001). Detecting vegetation leaf water content using reflectance in the optical domain. *Remote Sensing of Environment*, *77*(1), 22–33. https://doi.org/10.1016/S0034-4257(01)00191-2

Chappelle, E. W., Kim, M. S., & McMurtrey, J. E. (1992). Ratio analysis of reflectance spectra (RARS): An algorithm for the remote estimation of the concentrations of chlorophyll A, chlorophyll B, and carotenoids in soybean leaves. *Remote Sensing of Environment*, *39*(3), 239–247. https://doi.org/10.1016/0034-4257(92)90089-3

Coelho, R. C., Buffon, I., & Guerra, T. (2011). Influência do uso e ocupação do solo na qualidade da água: Um método para avaliar a importância da zona ripária. *Ambiente e Agua - An Interdisciplinary Journal of Applied Science*, *6*(1), 104–117. https://doi.org/10.4136/ambi-agua.177

Collins, H. P., Rasmussen, P. E., & Douglas, C. L. (1992). Crop Rotation and Residue Management Effects on Soil Carbon and Microbial Dynamics. *Soil Science Society of America Journal*, *56*(3), 783–788. https://doi.org/10.2136/sssaj1992.03615995005600030018x

Corbacho, C., Sánchez, J. M., & Costillo, E. (2003). Patterns of structural complexity and human disturbance of riparian vegetation in agricultural landscapes of a Mediterranean area. *Agriculture, Ecosystems & Environment*, *95*(2), 495–507. https://doi.org/10.1016/S0167-8809(02)00218-9

Corbane, C., Lang, S., Pipkins, K., Alleaume, S., Deshayes, M., García Millán, V. E., Strasser, T., Vanden Borre, J., Toon, S., & Michael, F. (2015). Remote sensing for mapping natural habitats and their conservation status – New opportunities and challenges. *International Journal of Applied Earth Observation and Geoinformation*, *37*, 7–16. https://doi.org/10.1016/j.jag.2014.11.005

Daily, G., Söderqvist, T., Aniyar, S., Arrow, K., Dasgupta, P., Ehrlich, P., Folke, C., Jansson, A., Jansson, B.-O., Kautsky, N., Levin, S., Lubchenco, J., Mäler, K.-G., Simpson, D., Starrett,

D., Tilman, D., & Walker, B. (2000). The Value of Nature and the Nature of Value. *Science*, *289*, 395–396. https://doi.org/10.1126/science.289.5478.395

Datt, B. (1998). Remote Sensing of Chlorophyll a, Chlorophyll b, Chlorophyll a+b, and Total Carotenoid Content in Eucalyptus Leaves. *Remote Sensing of Environment*, *66*(2), 111–121. https://doi.org/10.1016/S0034-4257(98)00046-7

De Luca, G., N. Silva, J. M., Cerasoli, S., Araújo, J., Campos, J., Di Fazio, S., & Modica, G. (2019). Object-Based Land Cover Classification of Cork Oak Woodlands using UAV Imagery and Orfeo ToolBox. *Remote Sensing*, *11*(10), 1238. https://doi.org/10.3390/rs11101238

Di Gennaro, S., Dainelli, R., Palliotti, A., Toscano, P., & Matese, A. (2019). Sentinel-2 Validation for Spatial Variability Assessment in Overhead Trellis System Viticulture Versus UAV and Agronomic Data. *Remote Sensing*, *11*. https://doi.org/10.3390/rs11212573

Dodkins, I., Aguiar, F., Rivaes, R., Albuquerque, A., Rodríguez-González, P., & Ferreira, M. T. (2012). Measuring ecological change of aquatic macrophytes in Mediterranean rivers. *Limnologica*, *42*(2), 95–107. https://doi.org/10.1016/j.limno.2011.09.001

Dubbini, M., Candiago, S., Remondino, F., De Giglio, M., & Gattelli, M. (2015). *Evaluating Multispectral Images and Vegetation Indices for Precision Farming Applications from UAV Images*. https://doi.org/10.13140/RG.2.1.3430.3527

D'Urso, G., Dini, L., Vuolo, F., Alonso, L., Guanter, L., & Agraria, F. D. (2004). RETRIEVAL OF LEAF AREA INDEX BY INVERTING HYPER-SPECTRAL, MULTI-ANGULAR CHRIS/PROBA DATA FROM SPARC 2003. *Undefined*. https://www.semanticscholar.org/paper/RETRIEVAL-OF-LEAF-AREA-INDEX-BY-INVERTING-DATA-FROM-D%E2%80%99Urso-Dini/37cf7ed4ce18ea08ea46498255782a2544d1643f

Dwire, K. A., Mellmann-Brown, S., & Gurrieri, J. T. (2018). Potential effects of climate change on riparian areas, wetlands, and groundwater-dependent ecosystems in the Blue Mountains, Oregon, USA. *Climate Services*, *10*, 44–52. https://doi.org/10.1016/j.cliser.2017.10.002

European Space Agency. (2015). *Sentinel-2 User Handbook*. *1*, 64.

Fairbanks, D. H. K., & McGwire, K. C. (2004). Patterns of floristic richness in vegetation communities of California: Regional scale analysis with multi-temporal NDVI. *Global Ecology and Biogeography*, *13*(3), 221–235. https://doi.org/10.1111/j.1466-822X.2004.00092.x

Gausman, H. W., Allen, W. A., Cardenas, R., & Richardson, A. J. (1971). Effects of Leaf Nodal Position on Absorption and Scattering Coefficients and Infinite Reflectance of Cotton Leaves, Gossypium hirsutum L.1. *Agronomy Journal*, *63*(1), 87–91. https://doi.org/10.2134/agronj1971.00021962006300010027x

Ghoussein, Y., Nicolas, H., Haury, J., Fadel, A., Pichelin, P., Abou Hamdan, H., & Faour, G. (2019). Multitemporal Remote Sensing Based on an FVC Reference Period Using Sentinel-2 for Monitoring Eichhornia crassipes on a Mediterranean River. *Remote Sensing*, *11*(16), 1856. https://doi.org/10.3390/rs11161856

Gómez-Sapiens, M., Schlatter, K. J., Meléndez, Á., Hernández-López, D., Salazar, H., Kendy, E., & Flessa, K. W. (2021). Improving the efficiency and accuracy of evaluating aridland riparian habitat restoration using unmanned aerial vehicles. *Remote Sensing in Ecology and Conservation*, *7*(3), 488–503. https://doi.org/10.1002/rse2.204

Gordo, O., & Sanz, J. (2010). Impact of climate change on plant phenology in Mediterranean ecosystems. *Global Change Biology*, *16*, 1082–1106. https://doi.org/10.1111/j.1365-2486.2009.02084.x

Gregory, S., Swanson, F., McKee, W., & Cummins, K. (1991). An Ecosystem Perspective of Riparian Zones. *Bioscience*, *41*. https://doi.org/10.2307/1311607

Gupta, R. K., Vijayan, D., & Prasad, T. S. (2003). Comparative analysis of red-edge hyperspectral indices. *Advances in Space Research*, *32*(11), 2217–2222. https://doi.org/10.1016/S0273-1177(03)90545-X

Han, X., Thomasson, J. A., Bagnall, G. C., Pugh, N. A., Horne, D. W., Rooney, W. L., Jung, J., Chang, A., Malambo, L., Popescu, S. C., Gates, I. T., & Cope, D. A. (2018). Measurement and Calibration of Plant-Height from Fixed-Wing UAV Images. *Sensors*, *18*(12), 4092. https://doi.org/10.3390/s18124092

He, K. S., Bradley, B. A., Cord, A. F., Rocchini, D., Tuanmu, M.-N., Schmidtlein, S., Turner, W., Wegmann, M., & Pettorelli, N. (2015). Will remote sensing shape the next generation of species distribution models? *Remote Sensing in Ecology and Conservation*, *1*(1), 4–18. https://doi.org/10.1002/rse2.7

Holmgren, P., & Thuresson, T. (1998). Satellite remote sensing for forestry planning—A review. *Scandinavian Journal of Forest Research*, *13*(1–4), 90–110. https://doi.org/10.1080/02827589809382966

Huylenbroeck, L., Laslier, M., Dufour, S., Georges, B., Lejeune, P., & Michez, A. (2020). Using remote sensing to characterize riparian vegetation: A review of available tools and perspectives for managers. *Journal of Environmental Management*, *267*, 110652. https://doi.org/10.1016/j.jenvman.2020.110652

International Journal of Applied Earth Observation and Geoinformation—Journal—Elsevier. (2012). https://www.journals.elsevier.com/journals.elsevier.com/international-journal-of-applied-earth-observation-and-geoinformation

Iverson, L. R., Graham, R. L., & Cook, E. A. (1989). Applications of satellite remote sensing to forested ecosystems. *Landscape Ecology*, *3*(2), 131–143. https://doi.org/10.1007/BF00131175

Khaliq, A., Comba, L., Biglia, A., Ricauda Aimonino, D., Chiaberge, M., & Gay, P. (2019). Comparison of Satellite and UAV-Based Multispectral Imagery for Vineyard Variability Assessment. *Remote Sensing*, *11*, 436. https://doi.org/10.3390/rs11040436

Kingra, P., Majumder, D., & Singh, S. P. (2016). Application of Remote Sensing and Gis in Agriculture and Natural Resource Management Under Changing Climatic Conditions. *Agricultural Research Journal*, *53*, 295–302. https://doi.org/10.5958/2395-146X.2016.00058.2

Kislik, C., Dronova, I., & Kelly, M. (2018). UAVs in Support of Algal Bloom Research: A Review of Current Applications and Future Opportunities. *Drones*, *2*(4), 35. https://doi.org/10.3390/drones2040035

Kislik, C., Genzoli, L., Lyons, A., & Kelly, M. (2020). Application of UAV Imagery to Detect and Quantify Submerged Filamentous Algae and Rooted Macrophytes in a Non-Wadeable River. *Remote Sensing*, *12*(20), 3332. https://doi.org/10.3390/rs12203332

Klemas, V. V. (2015). Coastal and Environmental Remote Sensing from Unmanned Aerial Vehicles: An Overview. *Journal of Coastal Research*, *315*, 1260–1267. https://doi.org/10.2112/JCOASTRES-D-15-00005.1

Lang, S., Mairota, P., Pernkopf, L., & Schioppa, E. P. (2015). Earth observation for habitat mapping and biodiversity monitoring. *International Journal of Applied Earth Observation and Geoinformation*, *37*, 1–6.

Loreau, M., Naeem, S., & Inchausti, P. (2002). Biodiversity & Ecosystem Functioning – Synthesis and Perspectives. In *Restoration Ecology—RESTOR ECOL* (Vol. 12).

Maingi, J. K., & Marsh, S. E. (2006). Composition, structure, and regeneration patterns in a gallery forest along the Tana River near Bura, Kenya. *Forest Ecology and Management*, *236*(2), 211–228. https://doi.org/10.1016/j.foreco.2006.09.006

Martin, R. V. (2008). Satellite remote sensing of surface air quality. *Atmospheric Environment*, *42*(34), 7823–7843. https://doi.org/10.1016/j.atmosenv.2008.07.018

Matese, A., Toscano, P., Di Gennaro, S. F., Genesio, L., Vaccari, F. P., Primicerio, J., Belli, C., Zaldei, A., Bianconi, R., & Gioli, B. (2015). Intercomparison of UAV, Aircraft and Satellite Remote Sensing Platforms for Precision Viticulture. *Remote Sensing*, *7*(3), 2971–2990. https://doi.org/10.3390/rs70302971

Messina, G., Peña, J. M., Vizzari, M., & Modica, G. (2020). A Comparison of UAV and Satellites Multispectral Imagery in Monitoring Onion Crop. An Application in the 'Cipolla Rossa di Tropea' (Italy). *Remote Sensing*, *12*(20), 3424. https://doi.org/10.3390/rs12203424

Mligo, C. (2017). Diversity and distribution pattern of riparian plant species in the Wami River system, Tanzania. *Journal of Plant Ecology*, *10*(2), 259–270. https://doi.org/10.1093/jpe/rtw021

Nezhad, M. M., Groppi, D., Laneve, G., Marzialetti, P., & Piras, G. (2018, April). *Oil Spill Detection Analyzing "Sentinel 2" Satellite Images: A PersianGulf Case Study*. The 3rd World Congress on Civil, Structural, and Environmental Engineering. https://doi.org/10.11159/awspt18.134

Nezhad, M. M., Heydari, A., Fusilli, L., & Laneve, G. (2019, April). *Land Cover Classification by using Sentinel-2 Images: A case study in the city of Rome*. The 4th World Congress on Civil, Structural, and Environmental Engineering. https://doi.org/10.11159/iceptp19.158

Oliveira, D., Fernandes, A., Rapazote, J., Teixeira, L., Brioso, R., Valente, C., Teixeira, F., & Medeiros, M. (2004). *A UTILIZAÇÃO DO "RIVER HABITAT SURVEY" NA GESTÃO AMBIENTAL DE ECOSSISTEMAS FLUVIAIS. POTENCIALIDADES E LIMITAÇÕES.* 15.

Pace, G., Gutiérrez-Cánovas, C., Henriques, R., Boeing, F., Cássio, F., & Pascoal, C. (2021). Remote sensing depicts riparian vegetation responses to water stress in a humid Atlantic region. *The Science of the Total Environment*, *772*, 145526. https://doi.org/10.1016/j.scitotenv.2021.145526

Piégay, H., Arnaud, F., Belletti, B., Bertrand, M., Bizzi, S., Carbonneau, P., Dufour, S., Liébault, F., Ruiz-Villanueva, V., & Slater, L. (2020). Remotely sensed rivers in the Anthropocene: State of the art and prospects. *Earth Surface Processes and Landforms*, *45*(1), 157–188. https://doi.org/10.1002/esp.4787

Pievani, T. (2014). The sixth mass extinction: Anthropocene and the human impact on biodiversity. *Rendiconti Lincei*, *25*(1), 85–93. https://doi.org/10.1007/s12210-013-0258-9

Pinter, Jr., Paul J., Hatfield, J. L., Schepers, J. S., Barnes, E. M., Moran, M. S., Daughtry, C. S. T., & Upchurch, D. R. (2003). Remote Sensing for Crop Management. *Photogrammetric Engineering & Remote Sensing*, *69*(6), 647–664. https://doi.org/10.14358/PERS.69.6.647

Pontoglio, E., Dabove, P., Grasso, N., & Lingua, A. M. (2021). Automatic Features Detection in a Fluvial Environment through Machine Learning Techniques Based on UAVs Multispectral Data. *Remote Sensing*, *13*(19), 3983. https://doi.org/10.3390/rs13193983

Postel, S., & Richter, B. (2003). *Rivers for Life: Managing Water For People And Nature*. Island Press.

Pu, R., Ge, S., Kelly, N. M., & Gong, P. (2003). Spectral absorption features as indicators of water status in coast live oak (Quercus agrifolia) leaves. *International Journal of Remote Sensing*, *24*(9), 1799–1810. https://doi.org/10.1080/01431160210155965

Quinn, J. M., Brown, P. M., Boyce, W., Mackay, S., Taylor, A., & Fenton, T. (2001). Riparian Zone Classification for Management of Stream Water Quality and Ecosystem Health1. *JAWRA*

Journal of the American Water Resources Association, *37*(6), 1509–1515. https://doi.org/10.1111/j.1752-1688.2001.tb03656.x

RedEdge User Manual (PDF)—Legacy. (n.d.). MicaSense Knowledge Base. Retrieved 24 February 2022, from https://support.micasense.com/hc/en-us/articles/215261448-RedEdge-User-Manual-PDF-Legacy

Revill, A., Florence, A., MacArthur, A., Hoad, S., Rees, R., & Williams, M. (2020). Quantifying Uncertainty and Bridging the Scaling Gap in the Retrieval of Leaf Area Index by Coupling Sentinel-2 and UAV Observations. *Remote Sensing*, *12*(11), 1843. https://doi.org/10.3390/rs12111843

Ribeiro, R., & Torgo, L. (2008). A comparative study on predicting algae blooms in Douro River, Portugal. *Ecological Modelling*, *212*(1–2), 86–91. https://doi.org/10.1016/j.ecolmodel.2007.10.018

Rocchini, D., Hernández-Stefanoni, J. L., & He, K. S. (2015). Advancing species diversity estimate by remotely sensed proxies: A conceptual review. *Ecological Informatics*, *25*, 22–28. https://doi.org/10.1016/j.ecoinf.2014.10.006

Rouse, J., Haas, R. H., Schell, J. A., & Deering, D. (1973). Monitoring vegetation systems in the great plains with ERTS. *Undefined*. https://www.semanticscholar.org/paper/Monitoring-vegetation-systems-in-the-great-plains-Rouse-Haas/fb2f60fe0fe2874e5cbf927a2556d719c32eac29

Rundle, S. (2002). Threats to the Running Water Ecosystems of the World. *Environmental Conservation*, *29*, 134–153. https://doi.org/10.1017/S0376892902000097

Sabater, S. (2008). Alterations of the Global Water Cycle and their Effects on River Structure, Function and Services. *Freshwater Reviews*, *1*(1), 75–88. https://doi.org/10.1608/FRJ-1.1.5

Santos, J. M., Godinho, F., Ferreira, M. T., & Cortes, R. (2004). The organisation of fish assemblages in the regulated Lima basin, Northern Portugal. *Limnologica*, *34*(3), 224–235. https://doi.org/10.1016/S0075-9511(04)80047-1

Shanmugapriya, P., Rathika, S., Ramesh, T., & Janaki, P. (2019). Applications of Remote Sensing in Agriculture—A Review. *International Journal of Current Microbiology and Applied Sciences*, *8*(01), 2270–2283. https://doi.org/10.20546/ijcmas.2019.801.238

Stimson, H. C., Breshears, D. D., Ustin, S. L., & Kefauver, S. C. (2005). Spectral sensing of foliar water conditions in two co-occurring conifer species: Pinus edulis and Juniperus monosperma. *Remote Sensing of Environment*, *96*(1), 108–118. https://doi.org/10.1016/j.rse.2004.12.007

ten Harkel, J., Bartholomeus, H., & Kooistra, L. (2019). Biomass and Crop Height Estimation of Different Crops Using UAV-Based Lidar. *Remote Sensing*, *12*(1), 17. https://doi.org/10.3390/rs12010017

Themistocleous, K. (2014). *The Use of UAV Platforms for Remote Sensing Applications: Case Studies In Cyprus*. *9229*, 92290S. https://doi.org/10.1117/12.2069514

Tilman, D., Clark, M., Williams, D. R., Kimmel, K., Polasky, S., & Packer, C. (2017). Future threats to biodiversity and pathways to their prevention. *Nature*, *546*(7656), 73–81. https://doi.org/10.1038/nature22900

Tilman, D., Reich, P. B., & Isbell, F. (2012). Biodiversity impacts ecosystem productivity as much as resources, disturbance, or herbivory. *Proceedings of the National Academy of Sciences of the United States of America*, *109*(26), 10394. https://doi.org/10.1073/pnas.1208240109

Tomsett, C., & Leyland, J. (2019). Remote sensing of river corridors: A review of current trends and future directions. *River Research and Applications*, *35*(7), 779–803. https://doi.org/10.1002/rra.3479

Torresani, M., Rocchini, D., Sonnenschein, R., Zebisch, M., Marcantonio, M., Ricotta, C., & Tonon, G. (2019). Estimating tree species diversity from space in an alpine conifer forest: The Rao's Q diversity index meets the spectral variation hypothesis. *Ecological Informatics*, *52*, 26–34. https://doi.org/10.1016/j.ecoinf.2019.04.001

Tucker, C. J., & Sellers, P. J. (1986). Satellite remote sensing of primary production. *International Journal of Remote Sensing*, *7*(11), 1395–1416. https://doi.org/10.1080/01431168608948944

van der Meij, B., Kooistra, L., Suomalainen, J., Barel, J. M., & De Deyn, G. B. (2017). Remote sensing of plant trait responses to field-based plant–soil feedback using UAV-based optical sensors. *Biogeosciences*, *14*(3), 733–749. https://doi.org/10.5194/bg-14-733-2017

Verbyla, D. L. (1995). *Satellite Remote Sensing of Natural Resources*. CRC Press.

Vieira, J. M. P., Duarte, A. A. L. S., & Pinho, J. L. S. (1998). *APLICAÇÃO DE UM MODELO DE QUALIDADE DA ÁGUA DO RIO CÁVADO AO ESTUDO DO IMPACTO DA CAPTAÇÃO DE ÁGUA DE AREIAS DE VILAR*. 17.

Vihervaara, P., Auvinen, A.-P., Poikolainen, L., Törmä, M., Ahlroth, P., Anttila, S., Böttcher, K., Forsius, M., Heino, J., Heliölä, J., Koskelainen, M., Kuussaari, M., Meissner, K., Ojala, O., Tuominen, S., Viitasalo, M., & Virkkala, R. (2017). How Essential Biodiversity Variables and remote sensing can help national biodiversity monitoring. *Global Ecology and Conservation*, *10*, 43–59. https://doi.org/10.1016/j.gecco.2017.01.007

Vitousek, P. M., Mooney, H. A., Lubchenco, J., & Melillo, J. M. (1997). Human Domination of Earth's Ecosystems. *Science*, *277*(5325), 494–499. https://doi.org/10.1126/science.277.5325.494

Wall, D. H., Palmer, M. A., & Snelgrove, P. V. R. (2001). Biodiversity in Critical Transition Zones between Terrestrial, Freshwater, and Marine Soils and Sediments: Processes, Linkages, and Management Implications. *Ecosystems*, *4*(5), 418–420.

Wallace, J. F., Caccetta, P. A., & Kiiveri, H. T. (2004). Recent developments in analysis of spatial and temporal data for landscape qualities and monitoring. *Austral Ecology*, *29*(1), 100–107. https://doi.org/10.1111/j.1442-9993.2004.01356.x

Westoby, M. J., Brasington, J., Glasser, N. F., Hambrey, M. J., & Reynolds, J. M. (2012). 'Structure-from-Motion' photogrammetry: A low-cost, effective tool for geoscience applications. *Geomorphology*, *179*, 300–314. https://doi.org/10.1016/j.geomorph.2012.08.021

Xu, J., Zhao, J., Wang, F., Chen, Y., & Lee, Z. (2021). Detection of Coral Reef Bleaching Based on Sentinel-2 Multi-Temporal Imagery: Simulation and Case Study. *Frontiers in Marine Science*, *8*. https://www.frontiersin.org/article/10.3389/fmars.2021.584263

Yadav, N. S., Kumar, A., & Sharma, M. P. (2014). Ecological Health Assessment of Chambal River using Water Quality Parameters. *Journal of Integrated Science and Technology*, *2*(2), 52–56.